Effects of Non-Axisymmetric Tip Clearance on Axial Compressor Performance and Stability

by

M.B. Graf, T.S. Wong, E.M. Greitzer, F.E. Marble,
C.S. Tan, H-W Shin, D.C. Wisler

GTL Report #228 September 1997

GAS TURBINE LABORATORY
MASSACHUSETTS INSTITUTE OF TECHNOLOGY
CAMBRIDGE, MASSACHUSETTS

Effects of Non-Axisymmetric Tip Clearance on Axial Compressor Performance and Stability

by

M.B. Graf, T.S. Wong, E.M. Greitzer, F.E. Marble,
C.S. Tan, H-W Shin, D.C. Wisler

GTL Report #228 September 1997

This research was sponsored by the Air Force Office of Scientific Research, Dr. James McMichael, Program Manager. Support for M. Graf was provided under the Air Force Research Aero Propulsion Technology (AFRAPT) Program.

EFFECTS OF NON-AXISYMMETRIC TIP CLEARANCE ON AXIAL COMPRESSOR PERFORMANCE AND STABILITY

M.B. Graf, T.S. Wong, E.M. Greitzer, F.E. Marble[1], C.S. Tan
Gas Turbine Laboratory
Massachusetts Institute of Technology
Cambridge, Massachusetts

H.-W. Shin, D.C. Wisler
Aero Technology Laboratories
GE Aircraft Engines
Cincinnati, Ohio

ABSTRACT

The effects of circumferentially non-uniform tip clearance on axial compressor performance and stability have been investigated experimentally and analytically. A theoretical model for compressor behavior with non-axisymmetric tip clearance has been developed and used to design a series of first-of-a-kind experiments on a four-stage, low speed compressor. The experiments and computational results together show clearly the central physical features and controlling parameters of compressor response to non-axisymmetric tip clearance.

It was found that the loss in stall margin was more severe than that estimated based on average clearance. The stall point was, in fact, closer to that obtained with uniform clearance at the maximum clearance level. The circumferential length scale of the tip clearance (and accompanying flow asymmetry) was an important factor in determining the stall margin reduction. For the same average clearance, the loss in peak pressure rise was 50% higher for an asymmetry with fundamental wavelength equal to the compressor circumference than with wavelength equal to one-half the circumference. The clearance asymmetry had much less of an effect on peak efficiency; the measured maximum efficiency decrease obtained was less than 0.4 percent compared to the 8% decrease in peak pressure rise due to the asymmetric clearance. The efficiency penalty due to non-axisymmetric tip clearance was thus close to that obtained with a uniform clearance at the circumferentially-averaged level.

The theoretical model accurately captured the decreases in both steady-state pressure rise and stable operating range which are associated with clearance asymmetry. It also gave a good

[1] Permanent address: California Institute of Technology, Pasadena, California.

description of the observed trends of (i) increasing velocity asymmetry with decreasing compressor flow, and (ii) decreasing effect of clearance asymmetry with decreasing dominant wavelength of the clearance distribution. The time resolved data showed that the spatial structure of the pre-stall propagating disturbances in the compressor annulus was well represented and that the stability limiting process could be linked to the unsteady structure of these disturbance modes.

The model was also utilized for parametric studies to define how compressor performance and stability is affected by the circumferential distribution of clearance, steady-state compressor pressure-rise characteristic, and system dynamic parameters. Sensitivity to clearance asymmetry was found to fall off strongly with the (asymmetry-related) reduced frequency and to increase with peak pressure rise and increasing curvature of the characteristic near the peak.

NOMENCLATURE

A_n Fourier coefficient

AR blade aspect ratio

b_x blade axial chord

B B - parameter, or a constant

B_m Fourier coefficient

f function

F force

h blade height

k characteristic peak pressure rise shift parameter

k_t throttle constant

L aerodynamic loss

m characteristic flow shift parameter

n spatial harmonic number

N number of compressor stages

P pressure

r radius

R degree of reaction

t time

T fluidic inertia parameter for a blade row

U rotor wheel speed

V velocity

x axial coordinate

Greek Symbols

β angle of characteristic peak line

γ blade stagger angle

δ perturbation quantity or boundary layer thickness

δ^* displacement thickness

ε tip clearance non-dimensionalized by chord

η efficiency

θ circumferential coordinate

λ inertia of fluid in rotor

μ inertia of fluid in compressor

ν endwall tangential force defect

ϕ flow coefficient

Φ velocity potential function

ρ density

τ blade row viscous loss time constant

ψ total-to-static pressure rise coefficient

ω radian frequency

Subscripts

1 at compression system inlet

2 at compressor face

3 at compressor exit

4 within plenum

5 at compression system exit

d design point

h,t hub, tip

i isentropic

IGV inlet guide vane

in at inlet

m hinge point

out	at outlet
p	peak point
r	rotor
s	stator
total	effective total length
ts	total-to-static
x	axial component

Superscripts

–	time mean value
~	cascade value

1. PROBLEM DESCRIPTION, MOTIVATION, AND SCOPE OF THE PAPER

It is well known that tip clearance has an important effect on the performance of axial compressors. Such aspects as peak pressure rise, peak efficiency, and stall margin all tend to be degraded as clearance is increased. Circumferential variations in tip clearance, such as those due to casing distortion or rotor eccentricity, present additional operating problems for gas turbine engines. Although it is recognized that such situations can affect performance in an adverse manner, almost all studies of tip clearance in the literature have focused on axisymmetric rather than non-axisymmetric clearance, so that the impact of the latter is much less understood.

It is useful to assign clearance non-uniformities into two broad categories: stationary and rotating asymmetries. Stationary asymmetries are stationary when viewed in the absolute (stationary) reference frame. They can be caused by relative displacement between the rotor and the casing (e.g. an off-centered rotor) or by deformation of the casing (e.g. casing ovalization). These two types of stationary asymmetries are illustrated in Figure 1. Compressors with such asymmetry have regions of small clearance and regions of large clearance relative to the designed clearance, although the average clearance remains unchanged from the design value. In contrast, rotating asymmetries exhibit unsteady circumferential clearance variations when viewed in the absolute frame. They can be generated by non-uniform rotor blade heights, by a whirling rotor, or by a "bowed rotor" in which there is mechanical bending or shaft deflection due to temperature non-uniformity. The focus of the present investigation is primarily on effects associated with stationary asymmetry, but a simple descriptive model for rotating asymmetry will be also be examined.

In Section 2 we present a qualitative description of the phenomena associated with compressor operation with non-axisymmetric clearance. As background to this, we will briefly summarize the effects of tip clearance on compressor performance and stability in an axisymmetric situation. Section 3 describes the modeling approach and gives selected numerical results to illustrate main trends. In Section 4 the approach to, and the design of, the experiments is discussed, followed by a short description of the compressor facility used to conduct the experiments in Section 5. The experimental results and the comparison with theory are then

presented in three stages: overall results (Section 6), time mean flow field (Section 7) and unsteady behavior and instability onset (Section 8). The parametric studies of Section 9 then show the influence of different design and system dynamic parameters on compressor sensitivity to non-axisymmetric clearance. Section 10 gives the summary and conclusions.

2. COMPRESSOR FLUID DYNAMIC FEATURES WITH ASYMMETRIC CLEARANCE

2.1. Background--Compressor Performance With Axisymmetric Tip Clearance

There is a large amount of data which show the effects of clearance on performance and stable flow range. An early compilation of experimental information which demonstrated the importance of rotor tip clearance on compressor pressure rise capability is that of Smith (1958). He showed that for a number of compressors with clearances between 1.5 and 8% of chord, a 1% increase in clearance produced approximately a 5% decrease in peak pressure rise. The trend illustrated by Smith (1958) has since been corroborated and extended by data from other sources including Koch (1981), Wisler (1985a), and Baghdadi (1995). Clearance effects on peak efficiency are well illustrated, also by Smith, in his landmark paper of 1970 (See also Koch and Smith, 1976) and by Wisler (1985b). Efficiency penalties range from 1 to 2 points for each 1% increase in the stage average clearance/blade height, depending upon the design.

2.2. Compressor Behavior with Asymmetric Tip Clearance

Although tip clearance asymmetry exists in all compressors to some extent (with the severity depending on both mechanical design and machine operating condition), published work on the effect of this phenomenon are much more sparse. Some data given by Freeman (1985) indicate that the stability margin is worsened compared to a machine with uniform clearance at the average level, and this seems anecdotally to be a general industry experience. However, there appears to be no rigorous methods for predicting the performance decrease and the flow field due to clearance asymmetry and it is thus of interest to define quantitatively how the stability and performance of a multi-stage compressor is affected by the distribution of clearance around the annulus.

In a compressor with asymmetric tip clearance, regions having smaller tip clearance produce increased pressure rise compared to those having larger clearance. resulting in a pressure rise and an axial velocity that vary around the circumference. The response of the compressor flow field to the clearance asymmetry can be viewed as somewhat analogous to a compressor operating with circumferential inlet distortion, although the flow non-uniformity is induced by a geometric variation within the compressor rather than by upstream conditions.

The approach taken here is to consider a compressor with non-axisymmetric clearance as a distribution of different compressors around the annulus, each with a pressure rise characteristic that corresponds to the local level of tip clearance. While this approach has a connection with the parallel compressor concept for circumferential inlet distortion, there is a difference in that locally the compressors are viewed as operating along *different* pressure rise characteristics.

We can illustrate the concept using Figure 2, which shows the total-to-static pressure rise characteristic for an axial compressor at three different, circumferentially-uniform, clearances. For reference, the values are based on a three-stage compressor with nominal clearance of 3% of chord, but the arguments to be given are quite general. Two situations are shown. In Figure 2a, the effect of clearance on the local pressure rise characteristic is a decrease in peak pressure rise. The peaks remain aligned at the same flow. In Figure 2b, a more general situation is shown in which not only the values of the peaks decrease but their locations have shifted to higher flow.

As a basic example, consider the compressor in Figure 2a with a cosine-shaped casing asymmetry having an amplitude equal to 2% of chord. The compressor will have minimum and maximum clearance-to-chord of 1% and 5% respectively. If we assume that the pressure rise behaves locally as with uniform clearance, the peak pressure rise will vary around the annulus from 10% below nominal to 10% above nominal and, at a particular circumferential position, will depend upon the level of clearance at that location.

For this compressor operating at peak pressure rise, the cosine-shaped clearance asymmetry will produce a circumferential variation in flow and pressure rise illustrated by the locus of points shown in Figure 3. At this condition, approximately half the points around the annulus are operating on positively-sloped portions of the local compressor characteristics and half are operating on the negatively-sloped portions. Figure 4 gives a different view of the situation and shows the magnitude and relative phase of the flow coefficient distribution at inlet to the compressor*.

* The results in Figures 3 and 4 were obtained using the model to be described in Section 3. Although the results are mainly meant to be illustrative, they provide a quantitative indication of the level of flow and pressure non-uniformity which can be expected.

3. MODELING APPROACH

With Section 2 as background, we now describe the modeling approach in more detail. The non-axisymmetric tip clearance model described (Graf, 1996) is an extension of the conceptual framework utilized by Hynes and Greitzer (1987) to assess effects of circumferentially non-uniform inlet flow on compressor performance and stability. It is to be emphasized strongly that the goal is to provide information about the overall behavior of the compressor and compression system, including stability and decrease in peak efficiency, rather than to capture the detailed fluid mechanics of the clearance flow. A schematic of the system considered is shown in Figure 5. There is a compressor which pumps flow to a plenum, which exhausts through an exit throttle. The compressor is assumed to have high hub-to-tip ratio so that the flow can be represented on a two-dimensional or meanline basis; the variations considered are in the axial and circumferential directions. The flow external to the compressor is taken as inviscid. The compressor and throttle are modeled as actuator disks, each of which has a nonlinear constitutive relation that includes a rudimentary description of blade row unsteady response. Finally, the compressor ducting is taken to be long enough so that there are no non-axisymmetric pressure field interactions with the inlet and exit duct terminations. [This is not a fundamental limitation of the model, but was done to (slightly) decrease algebraic complexity.] The relevant Mach numbers are assumed to be low enough that compressibility effects can be neglected in the compressor and in the ducts. Density changes in the plenum where effects of compressibility are important are related to pressure changes through an isentropic relationship.

The stability analysis consists of two distinct steps. The first involves the solution of the governing equations for the steady state background flow through the compression system. As is typical of hydrodynamic stability problems, this solution can be obtained whether or not such a flow would be stable in practice. The second step then involves adding a small perturbation to the background flow and determining from a linearized stability analysis whether or not such a disturbance grows or decays in time. The eigenvalues of the resulting system of linearized differential equations determine this and are the indications of stability. These steps will be

described briefly below.

3.1 Description of Steady Flow Analysis

In this section, we present only a summary of the analysis given in Appendix A. An equation for non-axisymmetric steady flow through a compressor with circumferentially uniform tip clearance has been given by Hynes and Greitzer (1987) as,

$$\frac{P_{exit} - P_{t,inlet}}{\rho U^2} = \psi(\phi) - \lambda \frac{d\phi}{d\theta} \tag{1}$$

The principal content of this equation is that the local pressure difference across the compressor (exit static minus inlet total) is given by the local uniform flow compressor pumping characteristic plus a correction to account for the fact that the flow in the rotors, which move through a circumferentially non-uniform flow, is unsteady. In Eq. (1) the compressor characteristic utilized is the axisymmetric non-dimensional total-to-static pressure rise coefficient, ψ, as a function of flow coefficient, ϕ. The parameter λ represents the inertia of the fluid in the rotor passages and is defined as

$$\lambda = \frac{b_x}{r \cos^2 \gamma} \tag{2}$$

We view the compressor with non-axisymmetric clearance as having a local pressure rise characteristic which is a function of the local tip clearance as well as the local flow coefficient. It is through modification of the characteristic that the effects of clearance asymmetry are included. The steady state performance of the compressor with non-uniform clearance is thus given by,

$$\frac{P_{exit} - P_{t,inlet}}{\rho U^2} = \psi(\phi, \varepsilon) - \lambda \frac{d\phi}{d\theta} \tag{3}$$

where ε is the non-dimensional tip clearance (normalized by rotor chord). The asymmetric background flow is obtained by solving Eq. (3), which is a nonlinear equation for ϕ as a function of θ, along with an equation which determines the annulus average flow through the compression system.

The background flow model (given in Appendix A and utilized in subsequent simulations)

is nonlinear, but it is helpful to present a simplified linear description to illustrate some basic parametric dependencies. For small variations from a uniform tip clearance in which $\delta\varepsilon = \delta\phi = 0$, Eq. (3) can be linearized to obtain the following expression for the steady flow non-uniformities in pressure and flow,

$$\frac{\delta P_{exit} - \delta P_{t,inlet}}{\rho U^2} = \frac{\partial \psi}{\partial \phi}\delta\phi + \frac{\partial \psi}{\partial \varepsilon}\delta\varepsilon - \lambda \frac{d\delta\phi}{d\theta} \tag{4}$$

In Eq. (4), δ signifies the circumferential non-uniformity and $\partial\psi/\partial\phi$ and $\partial\psi/\partial\varepsilon$ are the derivatives of the pressure rise characteristics with respect to axial flow coefficient and tip clearance. Since no losses are generated upstream of the compressor, the *total* pressure is circumferentially uniform at the inlet. Further, because the flow is assumed to exit the last stator axially, the *static* pressure at the compressor outlet is uniform. The quantities $\delta P_{t,inlet}$ and δP_{exit} are thus zero. Equation (4) thus reduces to a linear first order equation for $\delta\phi$ in terms of the (specified) clearance variation, $\delta\varepsilon$,

$$\lambda \frac{d\delta\phi}{d\theta} - \left(\frac{\partial \psi}{\partial \phi}\right)\delta\phi = \left(\frac{\partial \psi}{\partial \varepsilon}\right)\delta\varepsilon \tag{5}$$

The flow coefficient and clearance variation can be expressed in terms of Fourier series representations,

$$\delta\phi = \sum_{n=-\infty}^{\infty} A_n e^{in\theta} \quad , \qquad \delta\varepsilon = \sum_{n=-\infty}^{\infty} B_n e^{in\theta} \tag{6}$$

Substituting Eqs. (6) into (5), the variation in flow coefficient is found to be,

$$\delta\phi = \sum_{n=-\infty}^{\infty} B_n e^{in\theta} \cdot \left(\frac{\dfrac{\partial \psi}{\partial \varepsilon}}{in\lambda - \dfrac{\partial \psi}{\partial \phi}} \right) \tag{7}$$

Equation (7) shows the central features governing the flow non-uniformity. The axial velocity variations around the annulus depend on: (1) the harmonic content of the clearance variation (B_n), (2) the flow inertia parameter (λ), (3) the sensitivity of compressor pressure rise to axisymmetric clearance changes ($\partial\psi/\partial\varepsilon$), and (4) the local slope of the pressure rise characteristics ($\partial\psi/\partial\phi$). A more negatively sloped compressor characteristic, a larger inertia parameter, a higher harmonic

content of the clearance variation, and a decreased sensitivity to axisymmetric clearance changes all promote smaller variations in flow coefficient, and thus, presumably, create less of an adverse effect on overall compressor performance and stability.

3.2 Stability Analysis

Once the steady flow is obtained using Eq. (3), the stability of the compression system can be assessed by adding a small, arbitrary, unsteady perturbation to the steady flow and determining whether it grows or decays in time. The behavior of such perturbations is described by a coupled set of linearized equations (see Appendix A). Stability is linked to unsteady flow processes in the system and cannot be predicted using only steady state analyses.

In the present situation, there is an interaction between the steady flow non-uniformity and the unsteady disturbances. This interaction is included in the description of the upstream flow field and (most critically) the compressor, but is neglected in the downstream region. Physically, this corresponds to the neglect of the convection of mean flow vorticity by the disturbance velocity field. The goodness of this approximation has been demonstrated in several similar problems, namely circumferential inlet distortion (Hynes and Greitzer, 1987) and rotating stall (Lavrich, 1988), in both of which the velocity non-uniformities, and hence the demands on the approximations, are larger than encountered here. (Put another way, we adopt here an approximation for the downstream flow field impedance which has been shown to be adequate in situations which tax it more severely than the present application.) Further discussion of this point can be found in the above-mentioned two references.

Here it is primarily of interest to determine the condition (i.e. the annulus averaged pressure rise and flow) at which the compressor experiences the onset of rotating stall, which we associate with the growth of traveling wave-like disturbances. Development and growth of such disturbances has been reported by Haynes et al. (1994), Garnier et al. (1991), and was also observed in the present investigation.

As an example of the change in stability associated with clearance asymmetry, calculations

have been carried out for the three-stage compressor geometry mentioned previously. The configuration used had a mean clearance equal to 3% of the rotor chord and the nominal pressure rise characteristics shown in Figure 2a with the peaks of the pressure rise characteristics aligned. The clearance non-uniformity examined was cosine shaped. The amplitudes of the clearance non-uniformity about the uniform clearance ranged from 0% to 2% of the rotor chord, so the average clearance was always equal to 3% of chord although the level of clearance variation was varied. The results of the calculations are shown in Figure 6. As the amplitude of the asymmetric clearance increases from 0% to 2% of clearance/chord, the neutral stability point moves along curve "a" from point "0" to reduced pressure rise and higher flow coefficient at point "1". Compared to the uniform-clearance stability point, which is at the peak of the nominal characteristic at point "0", the flow coefficient at stall at point "1" has increased 1.4% and the pressure rise coefficient has decreased 3.7% for a 2% clearance asymmetry.

Figure 6 also contains results of calculations carried out to show the effect of shifting the peak pressure rise to a higher flow rate as tip clearance is increased (as in Figure 2b), since this is generally the trend seen in practice. Thus, for 2% clearance asymmetry, the peaks of the local pressure rise characteristics which make up the family shown in Figure 2b were shifted horizontally. The shift for this example corresponded to a 38% change in flow coefficient between the peaks for minimum and maximum clearances. The stability onset point now moves along segment (b) shown in Figure 6 to point 2; this gives an increase in flow coefficient at stall of 6.2% and a decrease in pressure rise coefficient of 5.8%. Once again, for all the calculations shown in Figure 6, *the mean clearance remains unchanged*, so the instability point is directly affected by the presence of the clearance asymmetry and the corresponding geometry-induced flow non-uniformity. The mechanism associated with the change in stall point will be discussed in greater detail in later sections.

4. EXPERIMENTAL DESIGN

To assess the basic theoretical framework, a set of experiments was designed and performed (Wong (1996)). This included compressor performance information at several different operating conditions, to assess the ability of the model to capture trends with compressor operating points, and the steady and unsteady flow field measurements.

The experiments were divided into two sets. In the first set, characteristics of the compressor with different axisymmetric clearance levels were obtained; these served as input to the analytical model. Three clearances were tested corresponding to 2%, 4%, and 6% of rotor chord (or equivalently to 1.5%, 2.9%, and 4.3% of annulus height). The performance of the 4% clearance/ chord configuration (or equivalently the 2.9% of annulus height clearance) served as the baseline or nominal case.

For reference, typical levels of clearance-to-annulus height in the rear block of compressors in modern commercial engines are about 1.5 to 2.0% (i.e. corresponding to 2.0 to 2.7% of rotor chord clearance). Average levels of clearance for the whole compressor are often quoted at about one percent; however, the rear block levels are larger than average because annulus heights are smaller. The low speed test geometry for our experiments is meant to model the middle and rear blocks of HP compressors, and clearance variations were used that bounded typical rear block engine levels.

The second set of experiments involved two different asymmetric clearance distributions. The analysis showed that the circumferential harmonic content of the clearance variation had a significant influence on the severity of asymmetric clearance effects, and the test series thus included configurations with a single lobe (first-harmonic) and a two-lobed (second-harmonic) clearance variation.

A summary of the axisymmetric and non-axisymmetric test configurations examined is provided in Table 1.

TABLE 1: SUMMARY OF TEST CASES

Test	Configuration	Average Clearance/Chord (Average Clearance/ Annulus Height)	Clearance Asymmetry/Chord (Clearance Asymmetry/ Annulus Height)	Wavelength of Asymmetry
	Axisymmetric			
1	small	2% (1.5%)	0	0
2	baseline	4% (2.9%)	0	0
3	large	6% (4.3%)	0	0
	Non-Axisymmetric			
4	one-lobed	4% (2.9%)	±2% (±1.4%)	circumference
5	two-lobed	4% (2.9%)	±2% (±1.4%)	one-half circumference

5. FACILITY DESCRIPTION

5.1 Low Speed Research Compressor

The experimental portion of this work was performed at the General Electric Aerodynamics Research Laboratory using the Low Speed Research Compressor (LSRC) test facility (Wisler, 1985a). A schematic of the facility is shown in Figure 7. Flow enters from the top through the cylindrical filter. A ring of eleven wall static pressure taps are located at the flow measurement plane shown in the figure; these serve to meter the flow rate. The air then passes through four compressor stages and exits into a plenum below the test floor, and through a circular throttle plate. The throttle plate moves vertically to change the effective exit area, regulating the flow through the machine. In the configuration tested, the compressor had a constant casing diameter of 1.524 meters (60 inches) and a hub-to-tip ratio of 0.85.

The blading used in this experiment is representative of a modern multi-stage blade design. The compressor has four identical (or repeating) stages. There are fifty-three inlet guide vanes. Each stage has fifty-four rotor blades and seventy-four stator blades. The blade Reynolds number was 3.5×10^5 based on rotor chord length and mid-span blade velocity. The tip Mach number was 0.2, so the flow can be considered incompressible for modelling purposes, and the degree of reaction was 67%. Some geometrical information is given in Table 2.

TABLE 2: FOUR-STAGE COMPRESSOR DESIGN PARAMETERS

IGV chord (mm)	84
IGV aspect ratio	1.36
IGV solidity	0.93
IGV midspan stagger	-3.5°
Rotor chord (mm)	91
Rotor aspect ratio	1.25
Rotor solidity	1.03
Rotor midspan stagger	47°
Stator chord (mm)	79
Stator aspect ratio	1.45
Stator solidity	1.22
Stator midspan stagger	14°

Steady state aerodynamic data were obtained using circumferential arrays of eleven casing static taps located at a flow measurement plane roughly 0.8 radii upstream of the IGV's, upstream of the first stage rotor, and at the compressor exit, and eleven mid-span Kiel probes placed circumferentially at the compressor inlet and exit. High response measurements were obtained from eight casing pressure transducers placed uniformly around the circumference just above the first stage rotor. Overall efficiency was obtained from shaft speed and torque measurements. Accuracy of the measurements was ±0.25% of full scale (2 psi) for all pressures, ±0.10% for pressure coefficient, ±0.12 % for overall flow coefficient, and ±0.15% for overall efficiency. Further details of the experimental configuration and instrumentation utilized in this study will be referred to as needed and a thorough description of the LSRC can be found in Wisler (1985a).

5.2 Description of Asymmetric Casing Geometry

The casing of the compressor is comprised of Plexiglas windows mounted on steel frames; there are twelve windows in each of four stages. These were moved radially using shims to provide the non-uniform clearance variation. The two clearance configurations for an individual stage are illustrated schematically in Figure 8, with each segment of the heavy lines corresponding to a window in each stage. Both the one-lobed and the two-lobed configurations had an average tip clearance equal to 4% of rotor chord (or equivalently 2.9% of rotor height), the same as the baseline configuration. In the experiments, the windows in all four stages were moved the same amount.

6. OVERALL RESULTS

6.1 Compressor Pressure Rise and Efficiency with Axisymmetric Tip Clearance

Figure 9a shows the overall total-to-static pressure rise characteristics of the compressor with different *axisymmetric* clearance values. Increased tip clearance causes a decrease in peak pressure rise and an increase in stalling mass flow. The clearance increase from 2% to 4% of rotor chord (or equivalently from 1.5% to 2.9% of blade height) caused considerably smaller changes than that from 4% to 6% (or equivalently from 2.9% to 4.3% of blade height), implying that the machine may be hub critical at tight clearance.

Efficiency characteristics for the three different levels of clearance are shown in Figure 9b. The efficiency is presented as changes from the peak (design point) value for the nominal clearance. The data indicate roughly two percent change in peak efficiency, a change in tip clearance of 2% rotor chord (or 1.5% blade height) .

6.2 Compressor Pressure Rise and Efficiency with Non-Axisymmetric Clearance

Compressor pressure rise characteristics with *non-axisymmetric* clearance are shown in Figure 10 as the data points. The axisymmetric results of Figure 9a are indicated by the dashed lines. The 4% of blade chord clearance (2.9% of blade height clearance) axisymmetric data (the middle dashed line) can be compared with the non-axisymmetric data, all of which is for an average clearance of 4% blade chord (2.9% blade height). There is a substantial degradation in pressure rise and flow range with the non-axisymmetric clearance.

Several other points can be noted. First, at high flow coefficients (say design point or above), the characteristics with non-axisymmetric clearance are close to those of the axisymmetric baseline; it is at low flow that the difference in performance between the configurations becomes large. Secondly, the degradation in compressor performance is less when the wavelength of the clearance is cut by half, as seen by comparing the two-lobed clearance asymmetry data with the one-lobed data in Figure 10. This is an effect of flow unsteadiness because the reduced frequency of the non-uniform flow increases by a factor of two, as will be discussed later. Finally, the

theoretical predictions, shown as solid lines in Figure 10, capture the effects of both asymmetry and reduced frequency, not only for pressure rise but also for flow coefficient at stall.

To assess in more detail the relative change in stall margin produced by the various clearance configurations, we compare differences in performance at the stall point using bar charts. These bar chart differences in stalling pressure rise coefficient and stalling flow coefficient are shown in Figures 11a and 11b respectively as deltas relative to the level of performance obtained for the baseline configuration with 4% blade chord axisymmetric clearance (2.9% blade height axisymmetric clearance). The left-hand side of the figure shows the performance for axisymmetric clearance and provides an indication of how changes in axisymmetric clearance affect stability. On the right side of the figure, the non-asymmetric clearance results are given. The differences in stall conditions for the two non-asymmetric configurations are of the same order as the changes arising from axisymmetric clearance variations alone. As an example, the stall point for the one-lobed asymmetry shows a decrease in peak pressure rise of more than 8% (see the right hand side of Figure 11a). Also, the stall point for the one-lobed asymmetry and a 4% blade chord (2.9% blade height) average clearance is closer to the stall point with the largest (6%) axisymmetric clearance (see Figure 10) than to the stall point with a 4% blade chord (2.9% blade height) axisymmetric clearance.

Measured compressor efficiencies for one-lobed and two-lobed non-axisymmetric configurations are shown in Figure 12 as the data points. Again, the data of Figure 9b for axisymmetric clearance are given as dashed lines. The peak efficiency for the two non-axisymmetric configurations are close to that for the baseline 4% blade chord (2.9% blade height) axisymmetric clearance configuration, indicating that clearance asymmetry has only a small impact on peak efficiency. This is consistent with the pressure rise characteristics which show only small differences between axisymmetric and non-axisymmetric clearance configurations at flows near design. Figure 12 also shows the theoretical predictions as the solid lines.

Figure 13 gives a comparison of the measured change in peak efficiency with axisymmetric and non-axisymmetric clearance and the value obtained from theory. The flow

conditions correspond to the peak efficiency points in Figure 12; these can be characterized as near or at design. Theory and data indicate that the circumferential variation in flow coefficient at near design conditions is much smaller than that near stall. Hence the overall efficiency penalty associated with clearance asymmetry, which depends quadratically on the amount the local compressor operating point differs from the peak efficiency point, is also small. Differences in efficiency, like those in pressure rise, thus only become appreciable away from design.

7. CIRCUMFERENTIAL DISTRIBUTION OF TIME-MEAN FLOW

Figure 14 shows the measured distribution of time-mean inlet axial velocity around the circumference of the compressor with the one-lobed clearance variation. The non-uniformity in axial velocity is seen to increase as the overall flow rate, and thus the slope of the compressor pressure-rise characteristic, decreases, as implied by the introductory discussion in Section 3. Further, if we regard the compressor as operating along a characteristic corresponding to the local level of clearance, the characteristics for axisymmetric clearance are farther apart near stall than near design. Both of these conditions cause flow field variations to be greater at low flow than at high flow. The results from theory, using the full nonlinear model, are also shown in Figure 14. It is seen that the theory captures the trend with flow as well as the shape of the axial velocity distribution.

The circumferential distributions of axial velocity for the two-lobed clearance configuration are shown in Figure 15. The circumferential length scale of the flow field variation has been reduced by a factor of 2 and the amplitude of the axial velocity variation has decreased. One way to view this behavior is by analogy with one-dimensional unsteady flow in a duct. For inviscid flow in a duct with a fixed driving pressure difference, the amplitude of the corresponding velocity perturbation decreases as the reduced frequency increases. The case of clearance non-axisymmetry corresponds roughly to a fixed variation in driving pressure as the length of the non-uniform region decreases. Thus, as the reduced frequency with respect to the non-uniformity increases, the amplitude of the axial velocity non-uniformity decreases. This effect can be seen by comparing the one-lobe and two-lobe data and predictions shown in Figures 13 and 14. Note that the two-lobed configuration is a more demanding test of the assumptions on which the model is based, yet the theory does capture the flow variation with acceptable accuracy.

The trends with operating point and lobe number are summarized in Figure 16, which shows the calculated and experimentally measured amplitudes of the flow variation at the design and near-stall points. For the one-lobed clearance distribution, the amplitude of the first and second harmonics of the variation are shown; for the two-lobed distribution, only the second harmonic is

considered. The data show an increase in amplitude as the overall flow is throttled from design conditions to near stall. The effect of flow unsteadiness mentioned above is also seen in comparing the results for one- and two-lobed asymmetries; higher harmonics result in increased unsteadiness as the rotor passes through the steady, spatially non-uniform velocity. Finally, note that the ratio of second harmonic to first harmonic is nearly twice as large near stall as at design, indicating a greater role of nonlinearity at the former conditions.

8. UNSTEADY RESULTS AND STABILITY

8.1 Circumferential Variation of Flow Unsteadiness

We now examine the unsteady flow processes that limit stability. With non-axisymmetric clearance, the steady flow field entering the compressor is non-axisymmetric. Figure 17 shows the shape of the least stable eigenmode of the compression system at several different times during a period. The wave changes shape as it travels around the annulus. The level of velocity fluctuation that a stationary sensor, such as a hot wire, would see thus differs at different points around the annulus because the unsteady waves which propagate on this background flow, i.e. the eigenmodes of the system, are non-sinusoidal. The example in Figure 17, which is based on the results with the single-lobed clearance, shows regions of large and small velocity amplitude roughly in quadrature with the clearance variation.

The regions of wave growth and decay can be directly linked to the sections of the annulus where the compressor is locally operating on either the unstable (positive slope) or stable (negative slope) portion of the pressure rise characteristic family. To see this, the calculated local value of the compressor characteristic slope ($\partial\psi/\partial\phi$) is shown in Figure 18. Comparison of Figures 17 and 18 shows that the region of positive slope corresponds to wave amplification while the region with negative slope produces attenuation. Gysling and Greitzer (1995) used the product of the pressure rise perturbation and mass flow perturbation, non-dimensionally $\delta\psi \cdot \delta\phi$ or $(\delta\phi^2) \cdot (\partial\psi/\partial\phi)$ as an indication of the unsteady energy input associated with dynamic instability. Wave growth or decay in a particular portion of the annulus is therefore associated with the addition or dissipation of perturbation mechanical energy by the compressor in that region. It is this mechanism which produces the change in stability associated with asymmetric clearance.

Figure 19 gives the spatial Fourier harmonic content of the traveling wave shown in Figure 17. As mentioned previously, the clearance asymmetry and resulting non-axisymmetric flow give the eigenmodes of the system a richer harmonic content; for a uniform flow the eigenmodes would each be associated with a single harmonic. In Figure 19 the first harmonic is dominant, but the second and third harmonic amplitudes are also a significant fraction of the first.

The calculated wave envelope shown in Figure 17 indicates that the amplitude of the velocity and pressure fluctuations will vary circumferentially. To investigate this, eight equally-spaced high-response pressure transducers were used to measure the level of unsteadiness around the compressor. The normalized root-mean-square values of the static pressure fluctuation measured above the first stage rotor operating at near stall are shown in the Figure 20, along with the corresponding pressure perturbation wave envelope calculated by the model. The relative level has been set by matching the peak values. The data indicate a widely varying fluctuation level, with the overall shape of the amplitude distribution agreeing well with the theoretical result. The trend of the maximum occurring near the edge of the large tip clearance region was also previously observed by Silkowski (1995).

8.2 Circumferential Position of Stall Onset

The theory asserts that the onset of stall is characterized by a rapid increase in perturbation amplitude due to the growth of an underdamped circumferentially traveling disturbance. Figure 21 shows time traces of the normalized unsteady pressure during a stall transient. These were obtained from transducers located above the first stage rotor with the baseline axisymmetric configuration. The abscissa is time in units of rotor revolutions and the ordinate is the circumferential positions of the eight transducers. Prior to stall, say for the ten revolutions before, all eight traces look roughly similar. Further, although the origin of the stall cell can also be traced back to a location near 250 degrees, once identified, the traveling wave grows similarly over the annulus, increasing in amplitude as it travels around.

With non-axisymmetric clearance, the results are quite different. Figure 22 shows the unsteady pressure data with the one-lobe configuration. As mentioned before (see Figure 20), the measured level of fluctuation is much higher at locations near 150 degrees and the stall cell can be traced back to approximately this location. The cell begins to grow at the 150 degree location and its amplitude increases as it reaches the 200 degree location. From 250 degrees back around to 50 degrees however, the amplitude decreases. There is thus disturbance growth at some locations and

decay at others, in line with previous arguments about the local value of the compressor characteristic slope and the unsteady energy input.

Examination of the stall cell inception location for different test runs of the baseline axisymmetric configuration and from the one-lobe asymmetric configuration is instructive. As a quantitative criteria, we define the inception points by the observation of a specific value of the RMS pressure fluctuation amplitude ($\delta\psi = 0.1$). A histogram of the stall cell inception locations defined in this manner is shown in Figure 23. The compressor with axisymmetric clearance does not appear to have a preferred location from which the stall cells emerge. Stall inception in the asymmetric compressor, however, always appears at the location where the flow field unsteadiness is the highest.

9. PARAMETRIC STUDY

The comparison of theory and experiment carried out gives confidence that the model can capture the essential physical phenomena and the relevant parametric trends. It is thus useful to describe a set of computations based on the model which were carried out to determine the effects of several design parameters on compressor stability with asymmetric tip clearance. The baseline used for this parametric study was the nominal characteristic shown in Figure 2 with parameters of the three-stage compressor studied by Haynes et al. (1994). Design variables were modified to assess the impact of: (a) compressor characteristic curvature, (b) compressor peak pressure rise, (c) clearance distribution, and (d) compressor\compression system coupling. A simplified linearized model of rotating clearance asymmetry is also described with the mathematical formulation given in Appendix C.

9.1 Effect of Compressor Characteristic Curvature

We first assess the effect on stability of changes in radius of curvature at the peak of the pressure rise characteristic. Generally, altering the peak radius of curvature changes the width of the compressor operating map. Three different levels of peak radius of curvature were examined: (i) baseline case, (ii) half the radius of the baseline case, and (iii) twice the radius of the baseline case. In all calculations the clearance asymmetry was cosine shaped with an amplitude which varied between 0 and 2% of rotor chord.

Figure 24 shows the locus of neutral stability points for the three different peak curvature cases. As the peak radius of curvature is reduced, the loss in stall margin increases for a given level of clearance asymmetry or peak shift; that is, characteristics with sharper peaks have increased sensitivity to clearance asymmetry.

To understand why the sensitivity is increased, we refer back to the discussion of Figure 2. Calculation of the locus of operating points at neutral stability (Figure 3) showed that approximately half the points around the annulus are in the positive slope region of the compressor map. As the radius of curvature is reduced (sharper peaks), the variations in pressure rise and slope encountered

around the annulus become greater. Regions of lower pressure rise and increased (steeper) positive slope are thus accessed, causing the onset of instability at a higher annulus averaged flow coefficient.

9.2 Effect of Compressor Peak Pressure Rise

The baseline three-stage compressor had a peak pressure rise of $\psi = 0.8$. To determine the effect of increasing the peak pressure rise, it is useful to think in terms of adding repeating stages to our baseline three-stage compressor. To make a comparison where only pressure rise has been altered, the compressor map width was set to be the same regardless of the number of stages. Increasing the peak height for fixed map width also results in a reduction of the peak radius of curvature. Figure 25 illustrates the pressure rise characteristics for the original three-stage compressor along with those for six and nine stage machines of the same map width. The highest, nominal, and lowest characteristics associated with a 2% clearance asymmetry are shown for each of the machines.

Figure 26 gives the loci of the movement of the neutral stability point for the three cases having different map heights. The results are normalized by the peak quantities to allow direct comparison. As the maximum pressure rise increases, the loss in stall margin (pressure rise and flow) also increases for a given level of clearance asymmetry or peak shift. This occurs for reasons directly analogous to those given in Section 9.1 for changes in peak curvature.

9.3 Effect of Tip Clearance Distribution

As shown both theoretically and experimentally, the number of lobes of the clearance asymmetry has a direct influence on performance penalty paid by the compressor. To further illustrate the impact of tip clearance geometry on stability, four different casing profiles were examined: (1) $cos(\theta)$, (2) $cos(2\theta)$, (3) $cos(4\theta)$, and (4) two 90 degree square notches (one above and one below the nominal clearance) separated by 90 degrees. The first three of these are continuous clearance variations which contain only a single spatial harmonic, while the fourth, in theory, contains an infinite number of harmonics. The average clearances of the four cases were specified to be the same and equal to the baseline.

The loci of neutral stability points for each of the clearance geometries is shown in Figure 27. As with the experiment, the clearance variations with the longest wavelength produced the greatest loss in stall margin, as seen by curve (4). For the discrete notches the movement of the neutral stability point is similar to that of the $cos(\theta)$ asymmetry because this non-uniformity has a dominant first harmonic. These trends are also similar to those obtained for the effects of the spatial extent of circumferential inlet distortions. That is, distortions with larger circumferential extent produced larger losses in stall margin.

The four clearance asymmetries in the above example were specified to maintain the same minimum, average, and maximum clearance. This is the way the experiments were carried out. This implies that the arc length of the two-lobed and four-lobed casings necessary to generate the asymmetry were longer than for the single-lobed casing. A more realistic scenario is that the casing arc length with asymmetric clearance would deviate little from the axisymmetric value. Thus, two-lobed and four-lobed asymmetries which had arc lengths the same as the single-lobed asymmetry were also examined. This means that the *average* clearance of the asymmetries *decreased* as the number of lobes increased. The loci of stall points for constant arc length cases with $cos(2\theta)$ (case 5) and $cos(4\theta)$ (case 6) are also shown in Figure 27. The lines for the constant arc length (cases (5) and (6)) lie above the baseline characteristic, because for constant arc length the average clearance decreases as lobe number increases.

9.4 Effect of Compressor\Compression System Coupling

A non-dimensional parameter which characterizes compression system dynamic behavior is

$$B = \frac{U}{2\omega L} \tag{8}$$

where L is the characteristic length of the compressor for one-dimensional (surge-type) oscillations and ω is the Helmholtz frequency of the system. We can write this parameter as the ratio of two characteristic frequencies in the form

$$B = \frac{(U/r)}{\omega}\left(\frac{r}{2L}\right) \tag{9}$$

where $r/2L$ represents the geometry of the compressor. The characteristic frequency of a propagating disturbance will scale with U/r, whereas the frequency associated with surge like disturbances does not scale with rotor speed, but rather, is related to the Helmholtz resonator frequency, ω. As the B-parameter is varied therefore, there will be some value at which surge-type frequencies and frequencies of the propagating disturbances come together, giving possibilities for resonance, increased sensitivity to perturbations, and hence a decreased stability. An analogous situation occurs with the asymmetry due to inlet distortion, where Chue *et al.* (1989) have presented a description of the physical mechanism for coupling the propagating and the surge-like disturbances. For small amplitude disturbances, this type of coupling will only occur if the mean flow is non-axisymmetric, so that the clearance non-uniformity is essential for its existence.

To investigate the effect of compressor-compression system coupling, computations using the cosine shaped clearance asymmetry were carried out with B-parameters from 0.05 to 0.8. The upper limit of 0.8 was chosen because B greater than this caused the zeroth ("surge like") mode to become unstable before the first ("stall like") mode.

Figure 28 shows the results for the 2% clearance asymmetry with the peaks of the characteristics first aligned and then shifted to 45 degrees. There is an increase in stalling flow coefficient over a range of values of B, with a broad peak at roughly $B = 0.4$.

9.5 Effect of Rotating Clearance Asymmetry

Throughout this investigation the focus has been on stationary clearance non-uniformities. A summary of the theoretical model is presented in Appendix C. It is useful, however, to give some discussion of the effect of rotating clearance asymmetries, which can also be encountered in practice, on the compressor flow field.

One difference between stationary and rotating asymmetries is the response of the flow fields upstream and downstream of the compressor. For the stationary asymmetry, the inlet static pressure is spatially non-uniform. At the compressor exit (assuming constant exit flow angle), the static pressure is circumferentially uniform. With a rotating asymmetry, the inlet total pressure

will also be non-uniform, and this flow distortion will rotate at some multiple of the shaft frequency. In addition, the exit of the compressor will also experience temporal variations in static pressure as the geometry-induced flow asymmetry rotates around the annulus, so a compressor with a rotating clearance asymmetry generates an unsteady flow at inlet and exit.

Appendix C describes a linearized model of the compressor response to a rotating clearance asymmetry similar to that presented in Section 3. One result is an expression for the axial flow variation induced by a rotating asymmetry,

$$\delta\phi_{rot} = \frac{\frac{\partial\psi}{\partial\varepsilon}\delta\varepsilon}{in(\lambda+\mu)+2i-\frac{\partial\psi}{\partial\phi}} \tag{10}$$

Comparing Eq. (10) with Eq. (7) for a stationary clearance asymmetry, it is observed that given the same clearance non-uniformity $\delta\varepsilon$, the flow non-uniformity will be smaller for the rotating asymmetry than for the stationary. This effect is due to the additional terms present in the denominator of Eq. (10) which account for the flow unsteadiness both external to and within the compressor. To illustrate the difference, Figure 29 gives the magnitude of the axial velocity variation, normalized by clearance variation, for stationary and rotating clearance asymmetries as a function of the compressor characteristic slope (i.e. operating point). The sensitivity to slope changes is substantially greater for the compressor with the stationary asymmetry.

We can also examine the axial distribution of the pressure field within the compressor as in Figure 30. The amplitude of the static pressure perturbations have been normalized by the inlet static pressure non-uniformity at stall with the rotating asymmetry. Results are shown for design and stall conditions.

As one might expect, the pressure disturbances decrease in amplitude through the machine but the change in amplitude with operating point is greater with the stationary asymmetry. Also, the static pressure disturbances go to zero at the compressor exit with the stationary asymmetry, while they remain non-zero for the rotating asymmetry, because the flow is unsteady at the compressor exit when the asymmetry rotates.

10. SUMMARY AND CONCLUSIONS

The effect of tip clearance asymmetry on multi-stage compressor performance and stability has been studied theoretically and experimentally.

1) A theoretical model was developed to describe and predict the steady and unsteady flow response of an axial compressor with asymmetric tip clearance. Clearance asymmetry was analyzed by viewing each circumferential location as operating along a pressure rise characteristic corresponding to the local level of clearance. The present work gives the first nonlinear treatment of the steady flow with clearance asymmetry and the first analysis of the effect on compressor stability.

2) Experiments to establish the impact of asymmetric tip clearance on multi-stage compressor performance and stability were designed and performed on a four-stage, low speed compressor. The theory was found to accurately describe the steady and unsteady behavior of the measured flow field. Specific findings were:

   - The theory accurately describes the steady and unsteady behavior of the measured flow field. The effects of clearance asymmetry and of reduced frequency were captured for pressure rise, for flow coefficient at stall, and for efficiency.

   - Non-axisymmetric tip cleraance resulting from casing distortion can significantly reduce the levels of compressor peak pressure rise and stable flow range relative to the levels obtained for an equivalent average axisymmetric clearance. As shown by both analysis and experiment, the decrease in stability (stall margin) for asymmetric clearance was closer to that obtained for averaged clearances equal to the maximum asymmetric clearance. Thus, peak pressure and stable flow range degrade in proportion to the increase in maximum level of the clearance asymmetry.

   - The reduction in *peak* efficiency due to clearance asymmetry was roughly equal to that obtained for an equivalent average axisymmetric clearance. Thus, peak efficiency degrades in proportion to the increase in average level of the clearance asymmetry.

   - The spatial harmonic content of the clearance asymmetry is an important factor in determining the severity of the impact on compressor performance and stability. Asymmetries with lower harmonics are more detrimental than asymmetries with higher harmonics. The most severe effects are produced by clearance asymmetries with dominant wavelength equal to that of the compressor circumference. This effect was also captured by the theory.

- Unsteady flow measurements with asymmetric clearance showed that the variation in RMS unsteadiness around the annulus is related to stall cell inception location and to the disturbance wave structure. The measured location of maximum flow field unsteadiness corresponded to the end of the large clearance sector and the theoretical location of maximum disturbance growth. The theoretical results imply that the stability of a compressor with clearance asymmetry can be linked to unsteady flow processes driven by the casing variation.

- For a given clearance non-uniformity, the circumferential variation in velocity is reduced if the asymmetry is rotating as opposed to stationary.

3) A parametric study was conducted to explore the effects of asymmetric clearance on compressor performance and stability. The results of the study were:

- There is an increased sensitivity to clearance asymmetry for compressors with characteristics that are steep, have high peak pressure rise, narrow map width, and sharp drop in pressure rise after the peak.

- Decreasing the wavelength of the clearance non-uniformity (i.e. increasing the reduced frequency) decreases the effect of clearance asymmetry on stall margin. Essentially all the benefit can be obtained with an asymmetry with four lobes.

- For a given compressor, sensitivity to clearance asymmetry is only a weak function of compressor\compression system coupling.

ACKNOWLEDGEMENTS

This work has been supported by the Air Force Office of Scientific Research, Dr. James McMichael, Program Manager. This support is gratefully acknowledged. Support for M. Graf was provided under the Air Force Research in Aero Propulsion Technology (AFRAPT) Program; this assistance is also appreciated. The authors would like to thank GE Aircraft Engines for support and permission to publish the results. We also acknowledge the indispensible efforts of Mr. Donald Menner of GE Aircraft Engines in helping carry out the experiments, and of Dr. C. Van Schalkwyk for facilitating implementation of the analytical and computational aspects of the work. Finally, we are most pleased to acknowledge the patience and understanding shown by Ms. D. Park to the authors during the manuscript preparation process.

REFERENCES

Baghdadi, S., "Modeling tip clearance effects in multi-stage axial compressors," ASME Paper, 95-GT-291, 1995.

Chue, R., Hynes, T. P., Greitzer, E. M., Tan, C. S., Longley, J. P., "Calculations of inlet distortion induced compressor flow field instability," *Int. J. Heat and Fluid Flow*, 1989, vol. 10, 211-223.

Freeman, C., "Effect of tip clearance flow on compressor stability and engine performance," von Karman Institute for Fluid Dynamics, Lecture Series 1985-05, 1985.

Garnier, V. H., Epstein, A. H., Greitzer, E. M., "Rotating waves as a stall inception indication in axial compressors," ASME *J. Turbomachinery*, 1991, vol. 113, 290-301.

Graf, M. B., "Effects of asymmetric tip clearance on compressor stability," Master's Thesis, Massachusetts Institute of Technology, Department of Aeronautics and Astronautics, 1996.

Greitzer, E. M., "The stability of pumping systems - The 1980 Freeman Scholar Lecture," ASME *J. Fluids Eng.*, 1981, vol. 103, 193-242.

Gysling, D. L., Greitzer, E. M., "Dynamic control of rotating stall in axial flow compressors using aeromechanical feedback," ASME *J. Turbomachinery*, 1995, vol. 117, 307-319.

Haynes, J. M., Hendricks, G. J., Epstein, A. H., "Active stabilization of rotating stall in a three-stage axial compressor," ASME *J. Turbomachinery*, 1994, vol. 116, 226-239.

Hynes, T. P., Greitzer, E. M., "A method for assessing effects of inlet flow distortion on compressor stability," ASME *J. Turbomachinery*, 1987, vol. 109, 371-379.

Koch, C. C., "Stalling pressure rise capability of axial flow compressor stages," ASME *J. Eng. Power*, 1981, vol. 103, 645-656.

Koch, C.C., Smith, L.H., "Loss sources and magnitudes in axial-flow compressors," ASME *J. Eng. Power*, 1976, vol. 98, 411-424.

Lavrich, P.L., "Time-resolved measurements of rotating stall in axial flow compressors," MIT Gas Turbine Laboratory Report No. 194, 1988.

Longley, J. P., "A review of non-steady flow models for compressor stability," ASME Paper, 93-GT-17, 1993.

McDougall, N. M., Cumpsty, N. A., Hynes, T. P., "Stall inception in axial compressors," ASME *J. Turbomachinery*, 1990, vol. 112, 116-125.

Silkowski, P.D., "Measurements of rotor stalling in a matched and a mismatched multistage compressor," MIT Gas Turbine Laboratory Report No. 221, 1995.

Smith, L. H., Jr., "The effect of tip clearance on the peak pressure rise of axial-flow fans and compressors," ASME Symposium on Stall, 1958, 149-152.

Smith, L. H., Jr., "Casing boundary layers in multistage axial flow compressors," in *Flow Research on Blading*, edited by L. S. Dzung, Elsevier Publishing Co., 1970.

Wisler, D. C., "Loss reduction in axial-flow compressors through low-speed model testing," ASME *J. Eng. Gas Turbines and Power,* 1985a, vol. 107, 354-363.

Wisler, D. C., "Advanced compressor and fan systems," General Electric Aircraft Engine Business Group Publication, Cincinnati, Ohio, 1985b.

Wong, T. S., "Effects of asymmetric tip clearance on compressor performance and stability," Master's Thesis, Massachusetts Institute of Technology, Department of Aeronautics and Astronautics, 1996.

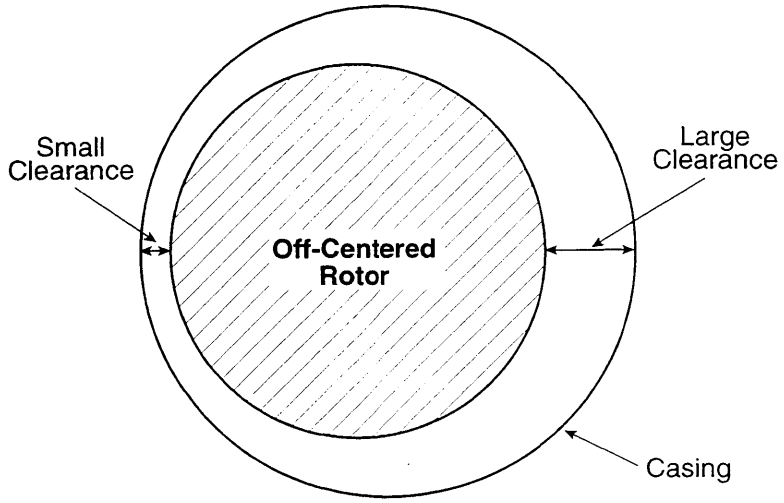

(a) Off-centered rotor

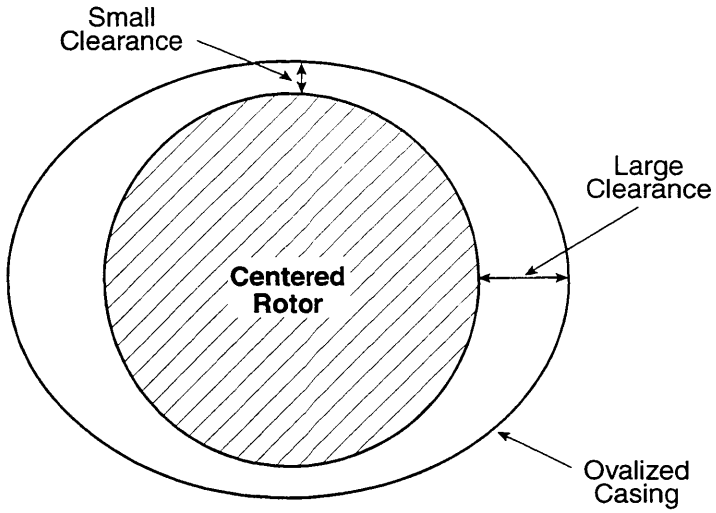

(b) Ovalized casing

Fig. 1: Non-axisymmetric tip clearance caused by: (a) off-centered rotor, and (b) ovalized casing.

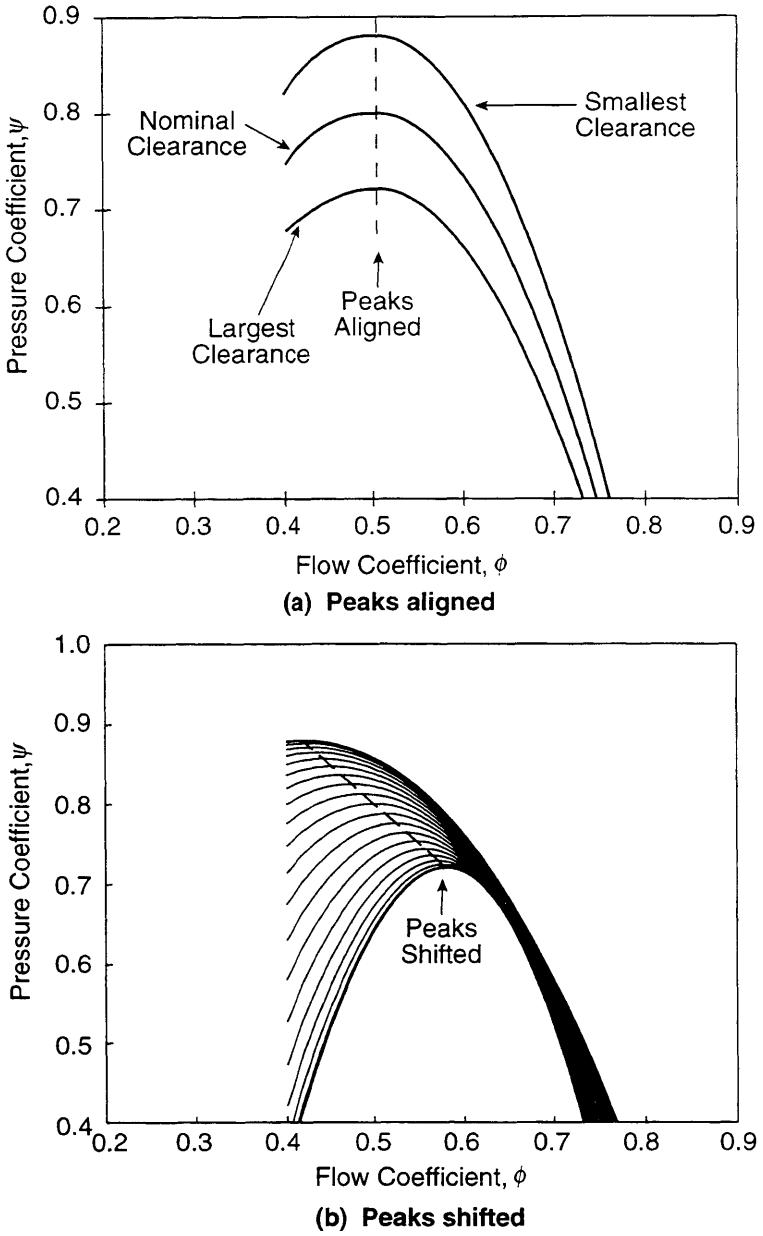

Fig. 2: Possible pressure rise characteristics for an axial compressor at three different clearances: (a) peaks in pressure aligned, (b) peaks in pressure shifted.

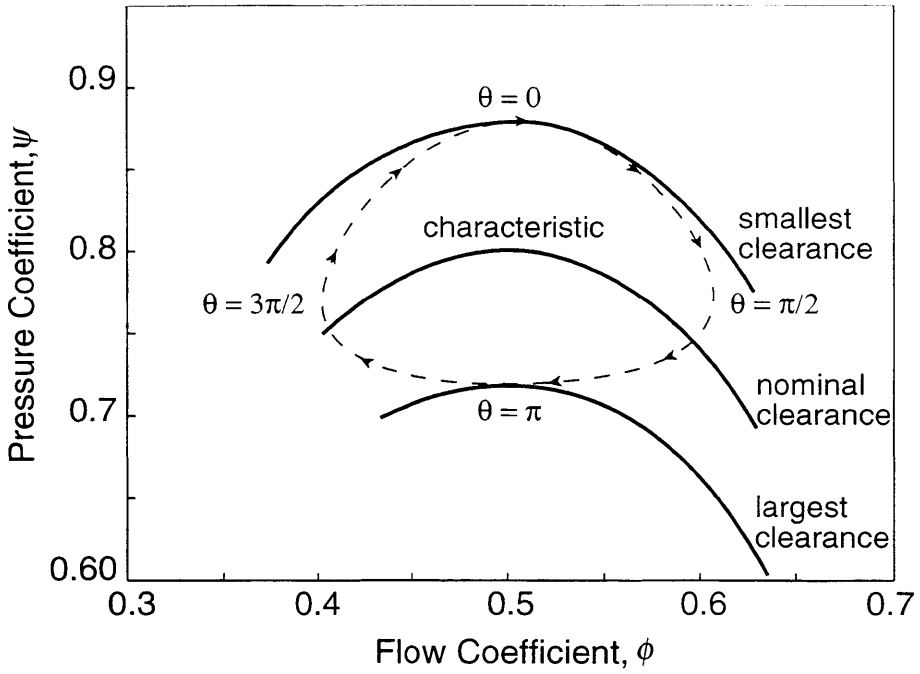

Fig. 3: Locus of operating points around the annulus for a compressor with non-axisymmetric clearance variation operating at peak pressure rise conditions.

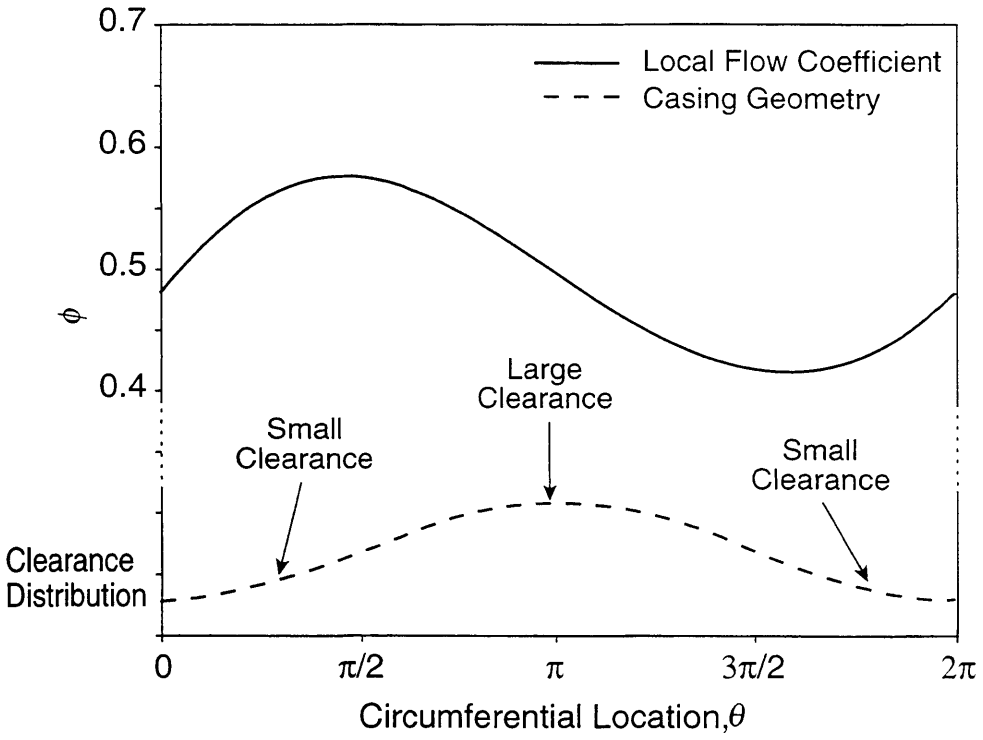

Fig. 4: Distribution of inlet flow coefficient around the annulus of the compressor with non-axisymmetric tip clearance, characteristics of Fig. 2a, operating at peak pressure.

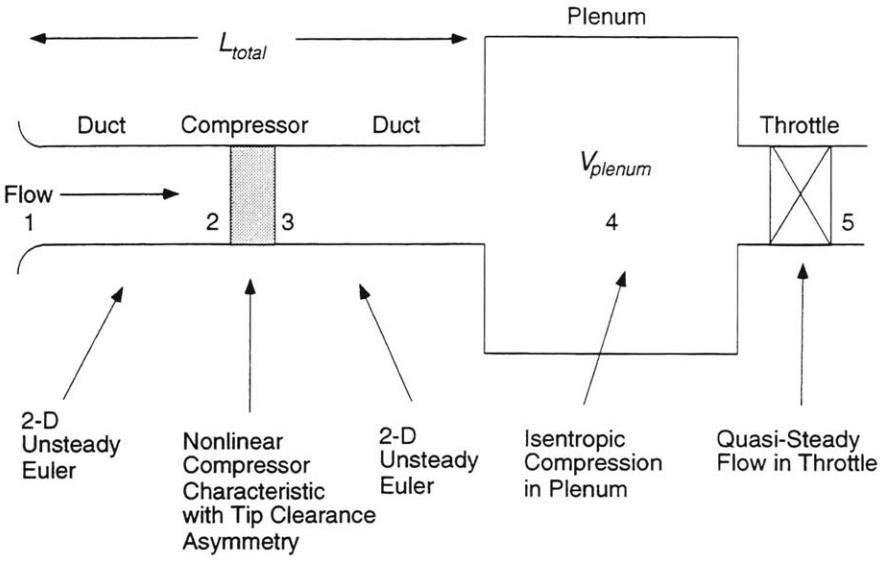

Fig. 5: Schematic of compression system.

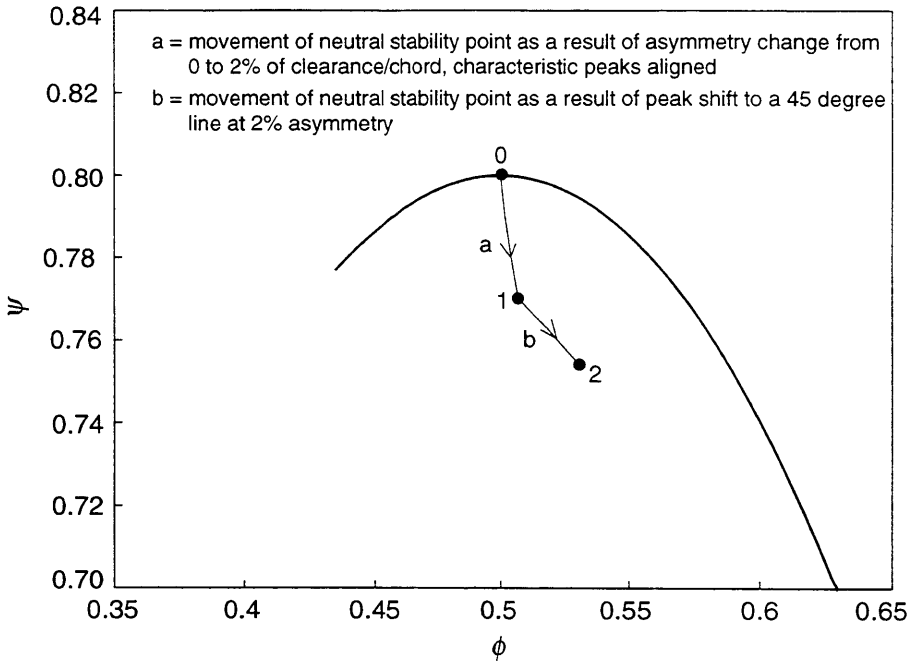

Fig. 6: Locus of instability points for different levels of clearance asymmetry.

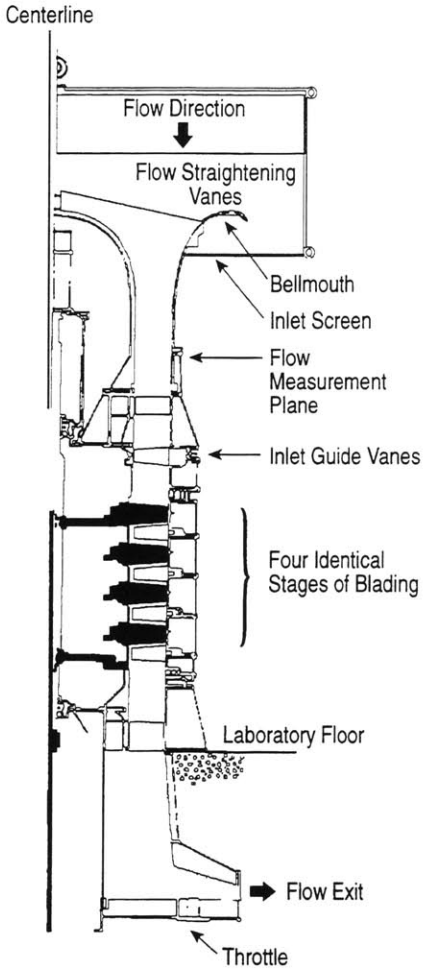

Fig. 7: Schematic of the GE LSRC test facility.

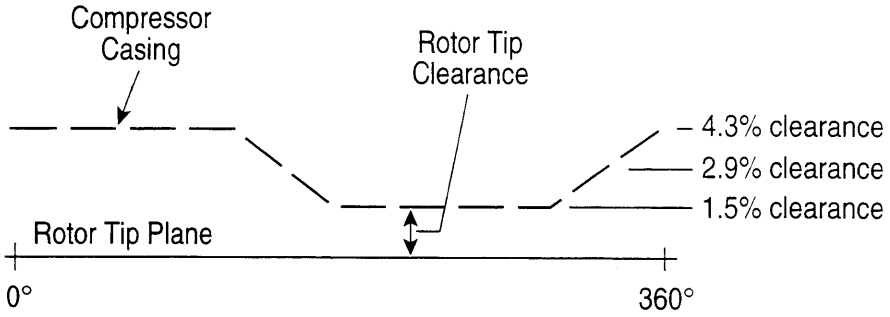

a) One-Lobed Clearance Asymmetry

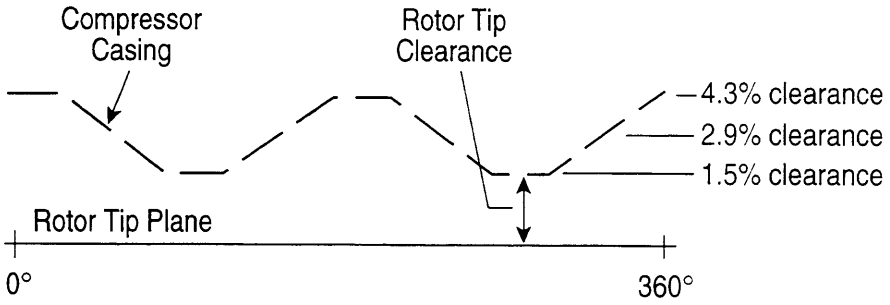

b) Two-Lobed Clearance

Fig. 8: Clearance geometries tested in the LSRC.

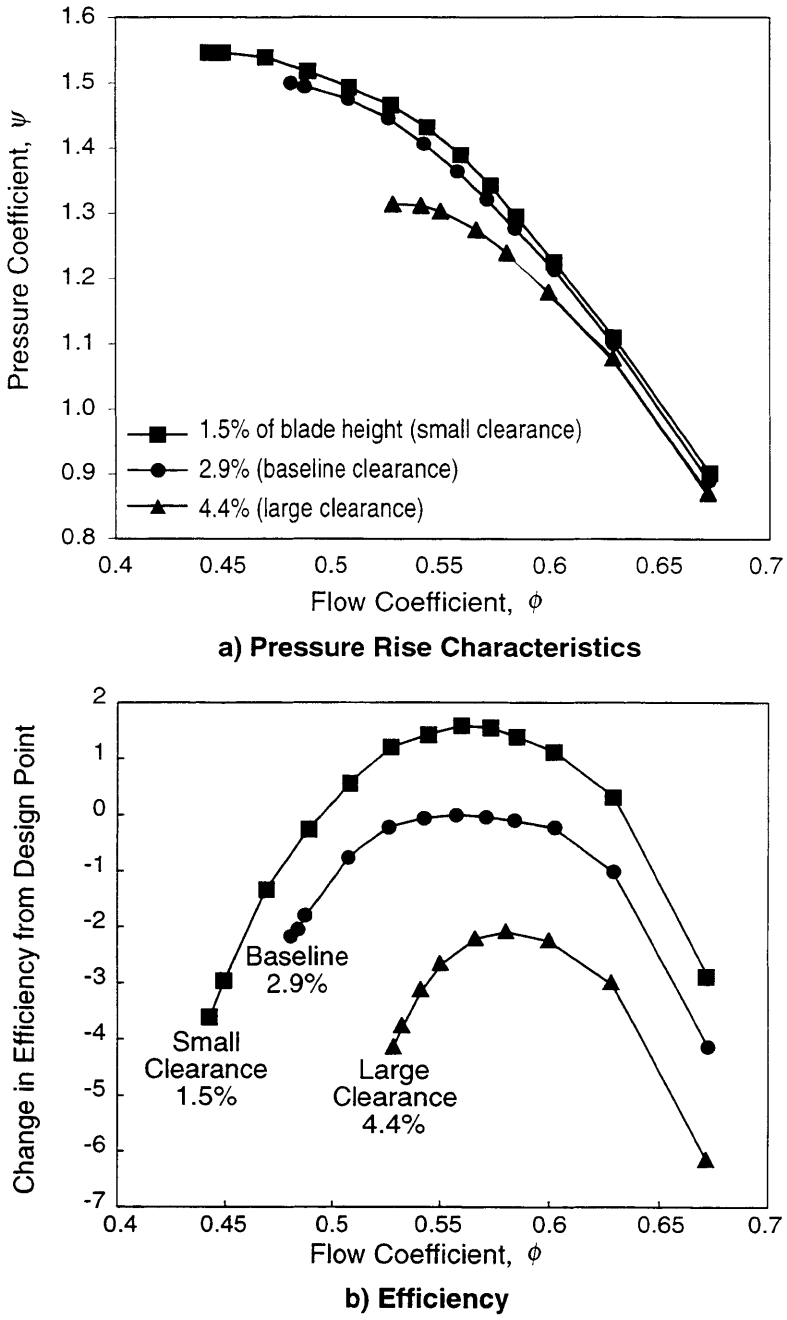

Fig. 9: Measured compressor performance with different axisymmetric clearances.

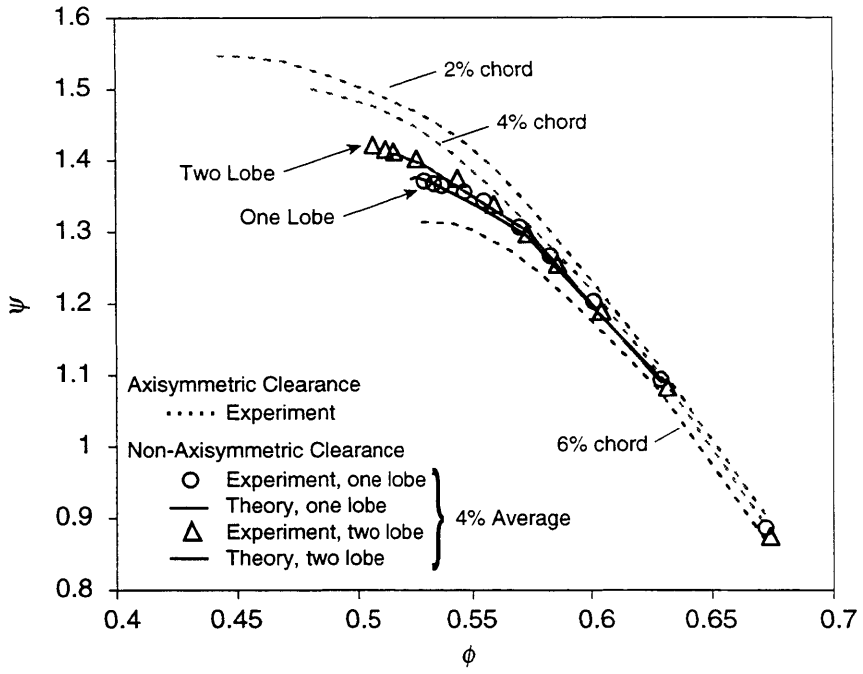

Fig. 10: Pressure rise characteristics with non-axisymmetric clearance.

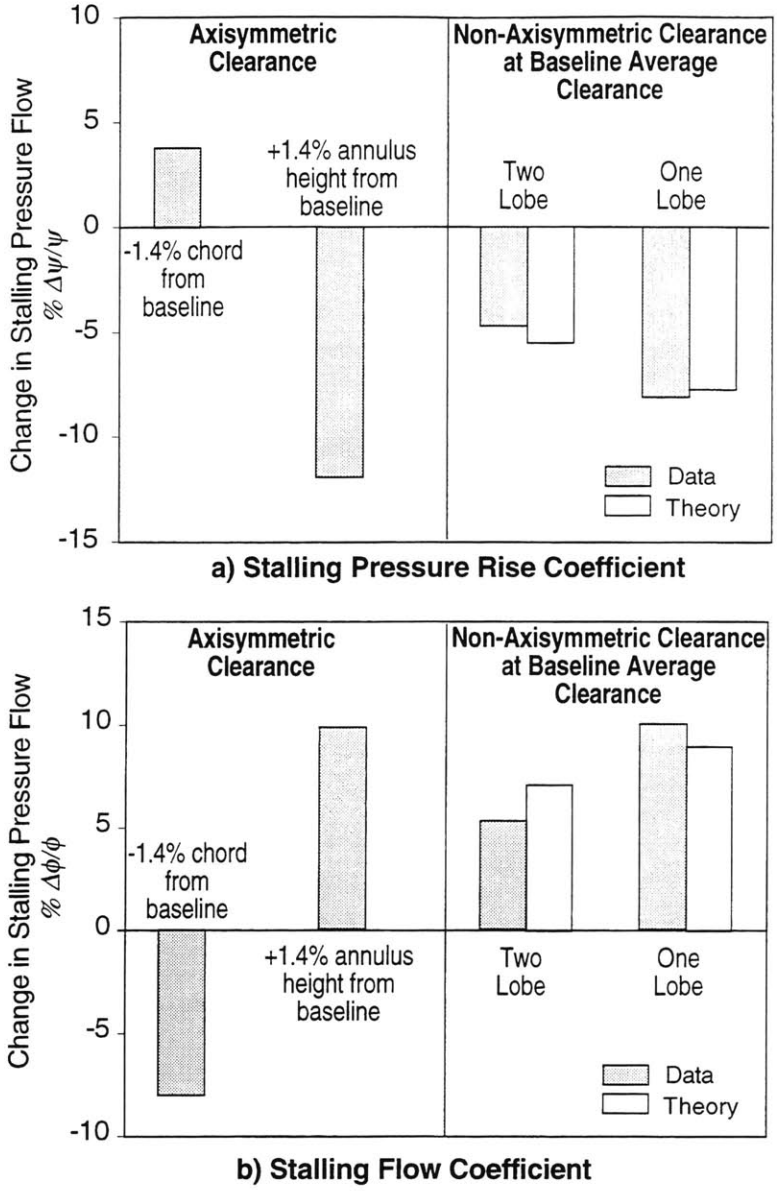

Fig. 11: Changes in stalling pressure rise and flow coefficient with axisymmetric and non-axisymmetric clearance: (a) stalling pressure rise, (b) stalling flow coefficient.

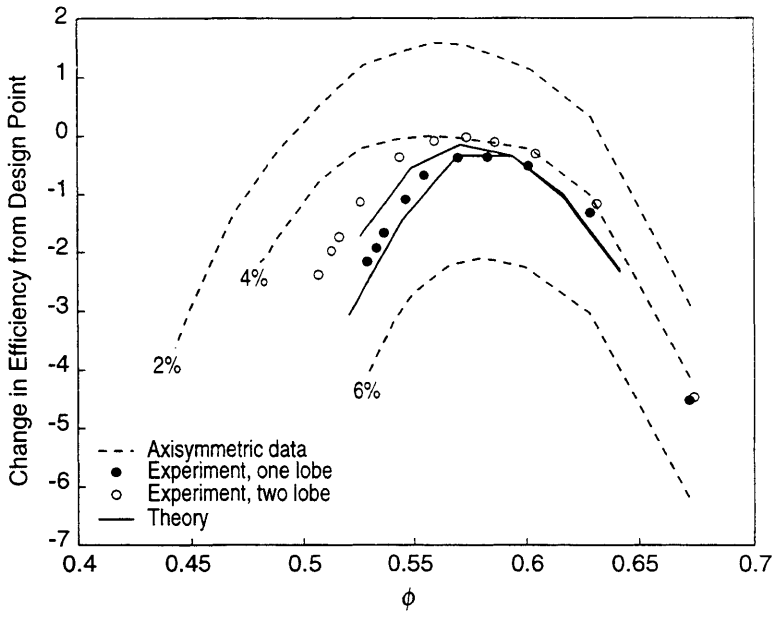

Fig. 12: Compressor efficiency with asymmetric clearance.

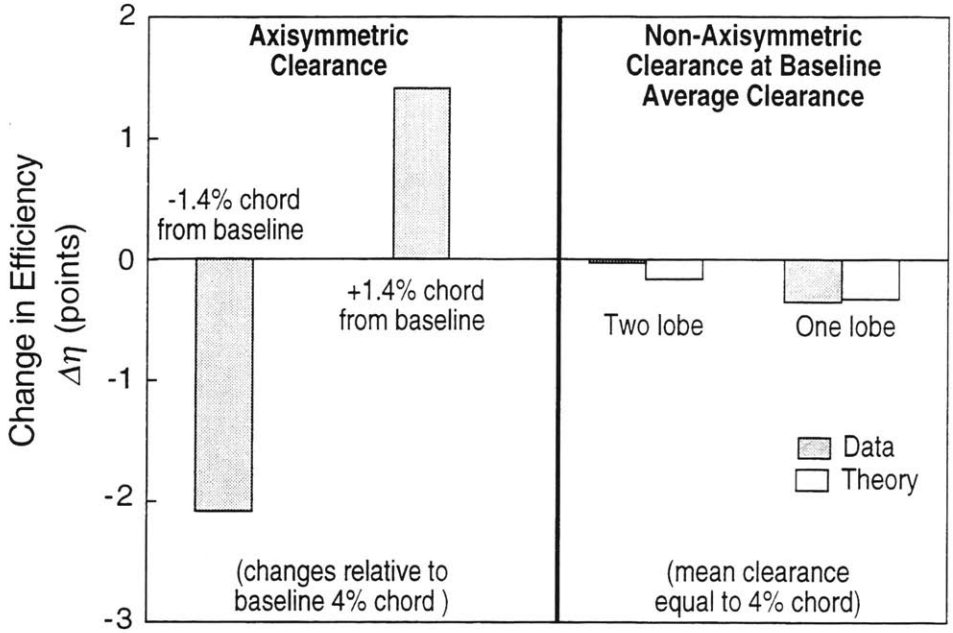

Fig. 13: Changes in peak efficiency with asymmetric clearance. (Flow conditions corresponding to peak efficiency points in Fig. 12.)

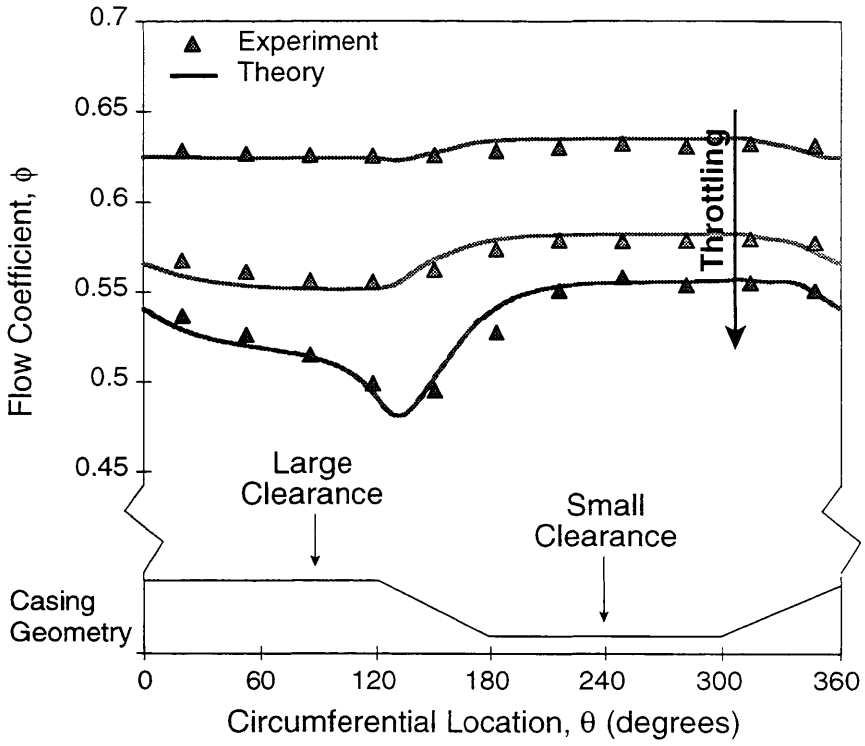

Fig. 14: Flow coefficient distribution with one-lobed asymmetry.

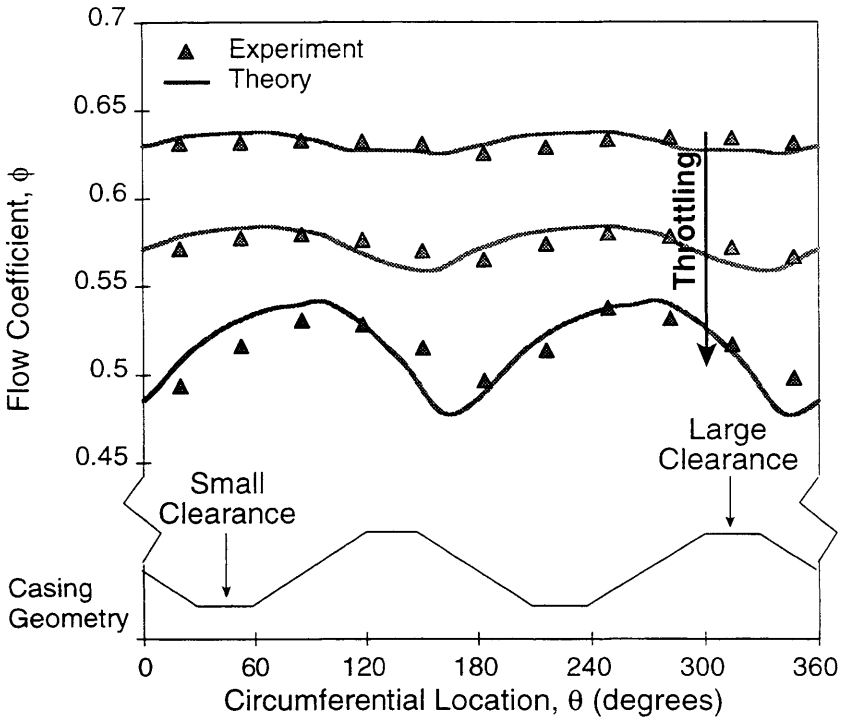

Fig. 15: Flow coefficient distribution with two-lobed asymmetry.

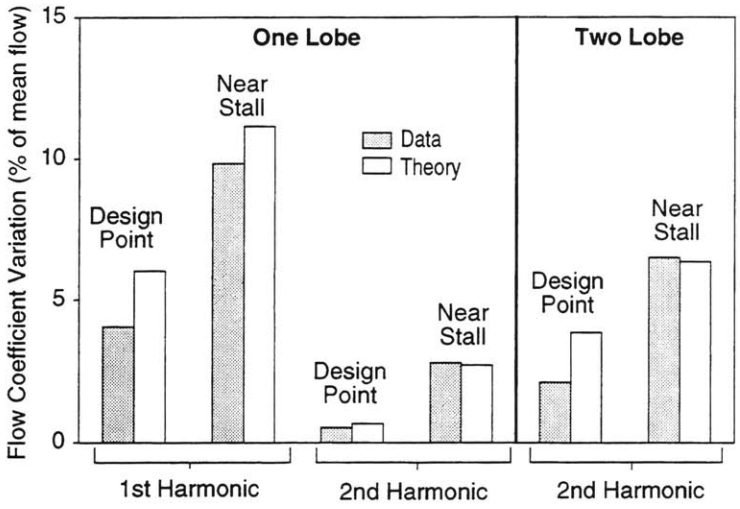

Fig. 16: Spatial harmonics of steady flow variation.

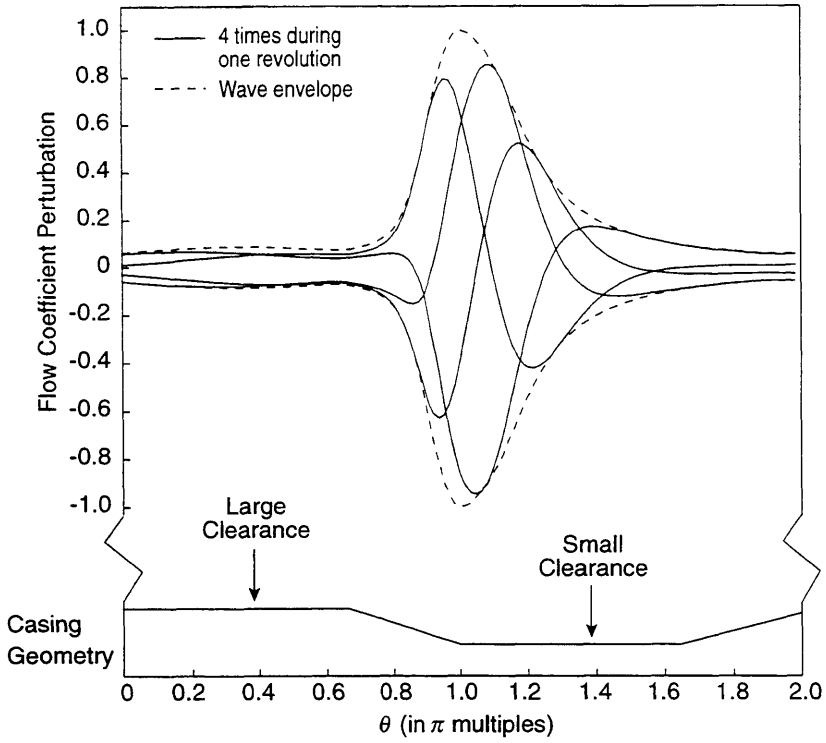

Fig. 17: Traveling wave disturbance at different times (least stable eigenmode of the compression system) at neutral stability point.

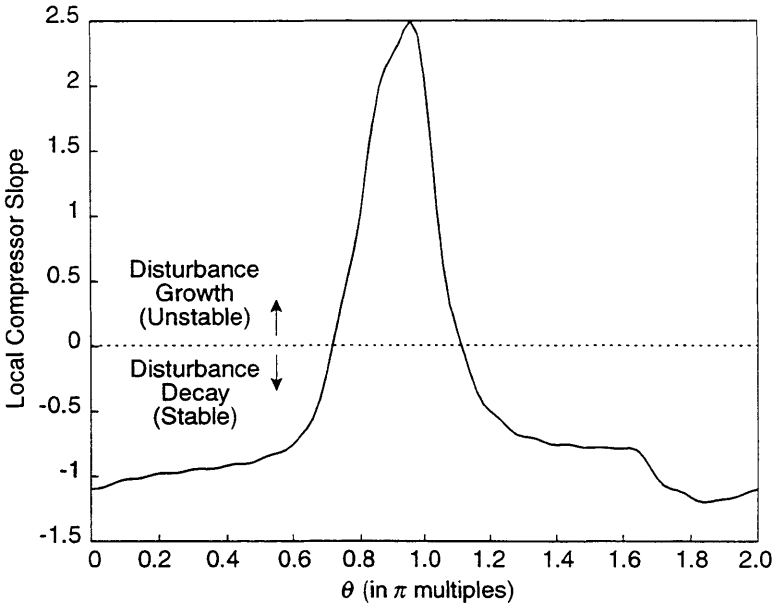

Fig. 18: Predicted variation in pressure rise characteristic slope; conditions corresponding to those in Figure 17.

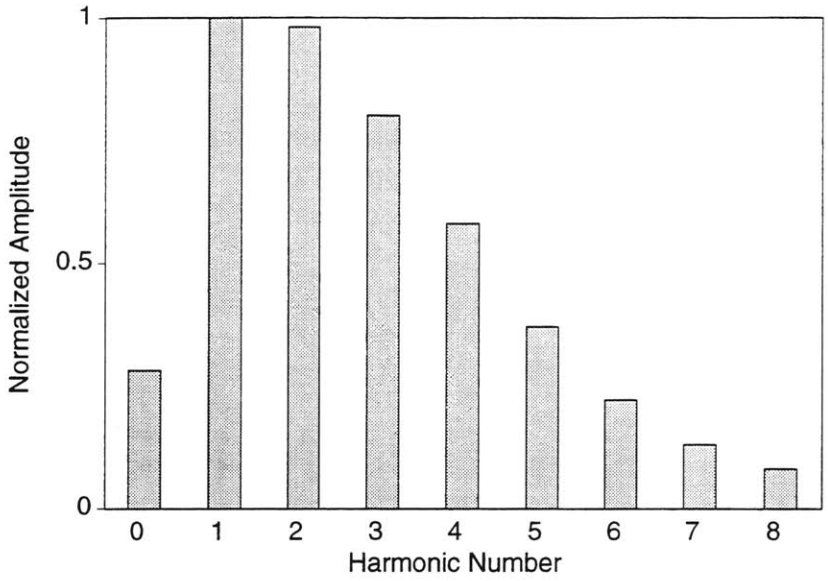

Fig. 19: Spectral content of least stable eigenmode at neutral stability; conditions corresponding to Figure 17.

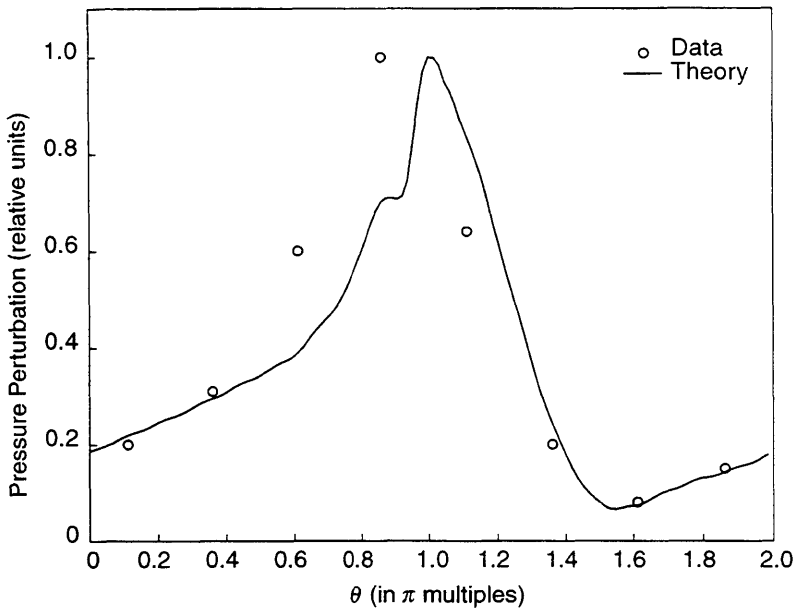

Fig. 20: Amplitude of static pressure disturbance above the first stage rotor.

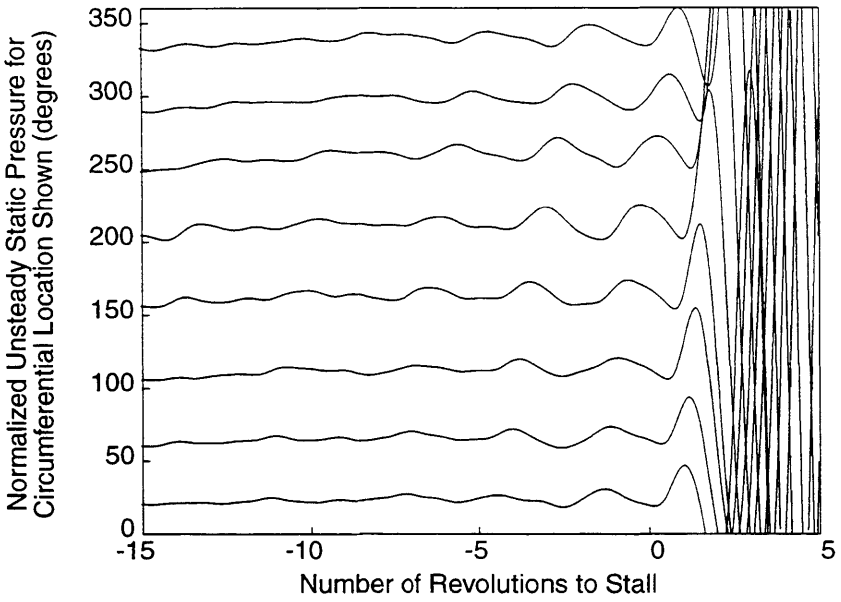

Fig. 21: Time traces of static pressure measured with baseline axisymmetric clearance.

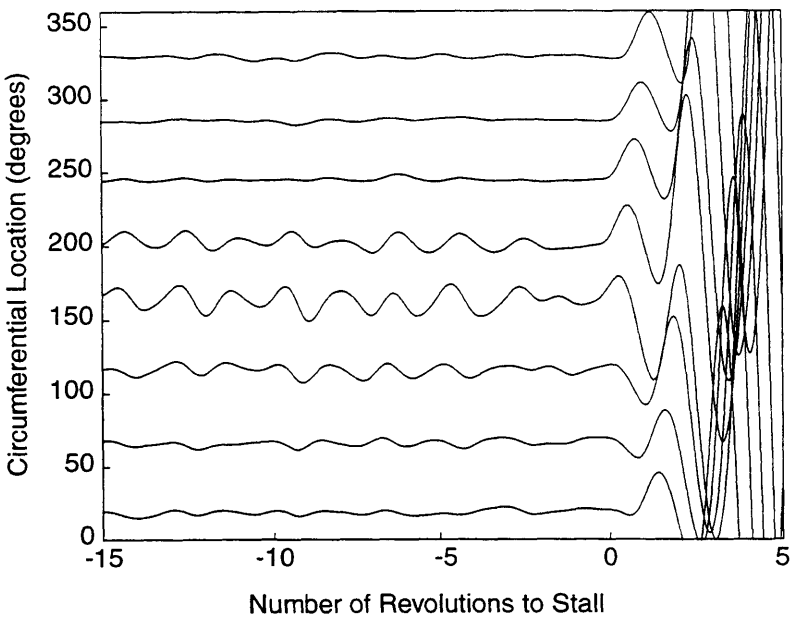

Fig. 22: Time traces of static pressure measured with single-lobed asymmetric clearance.

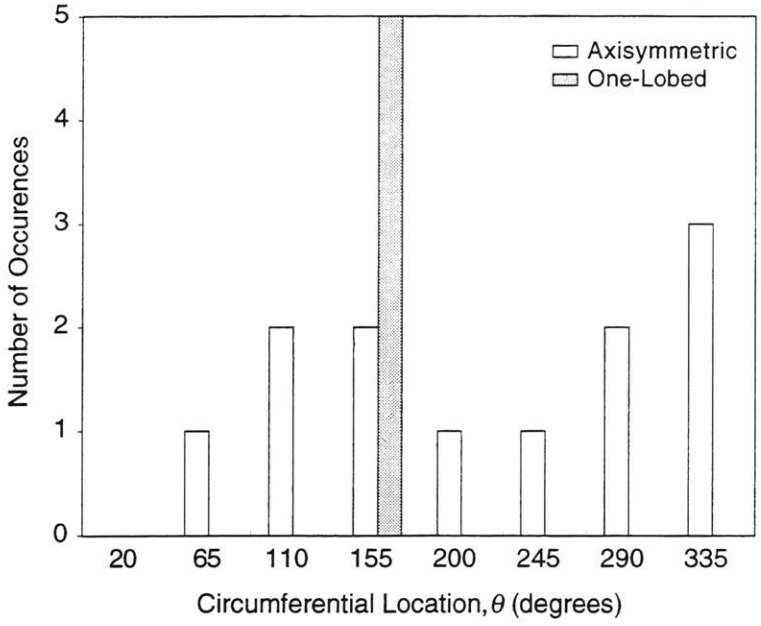

Fig. 23: Histogram of rotating stall inception locations based on criteria of $\delta\psi = 0.1$.

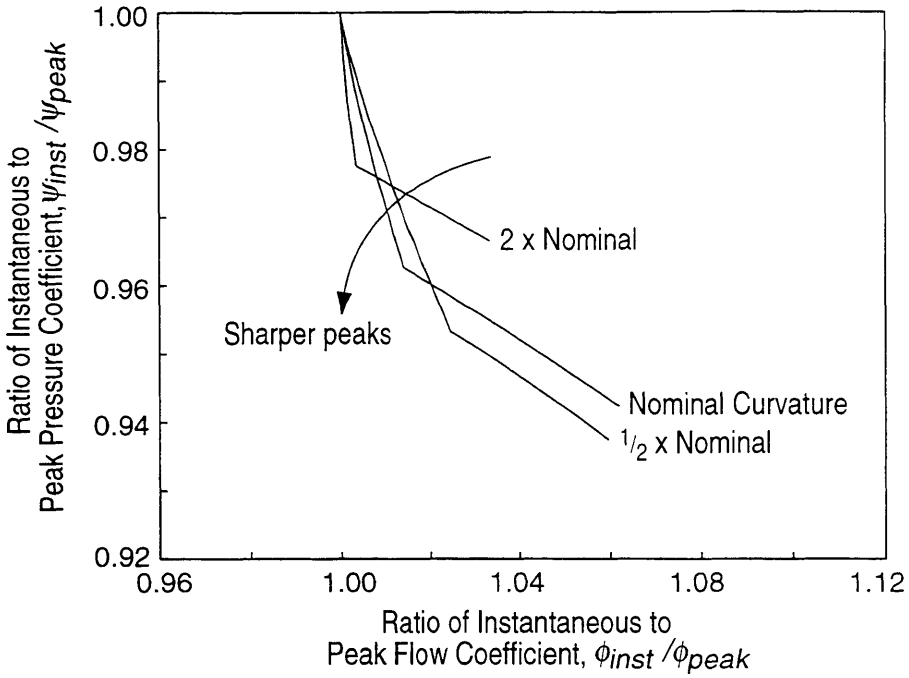

Fig. 24: Effect of compressor characteristic curvature (at the peak) on instability point.

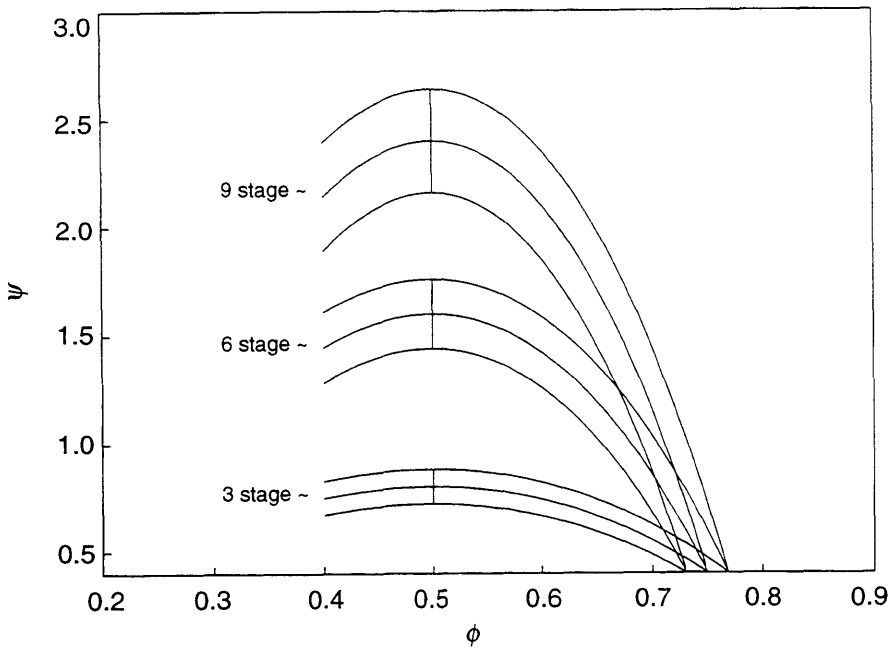

Fig. 25: Pressure rise characteristic families having different peak pressure rise.

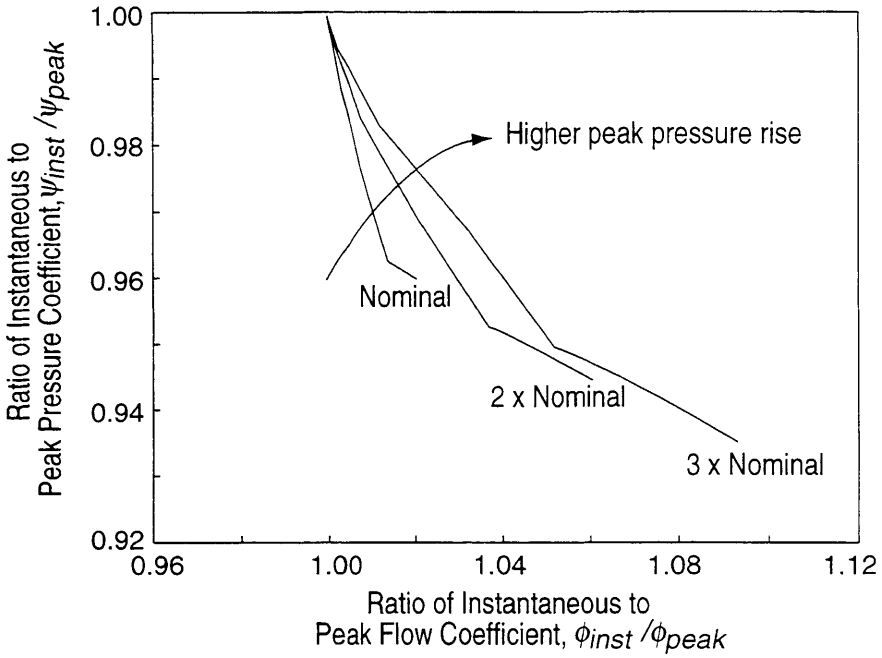

Fig. 26: Effect of peak pressure rise on instability point movement.

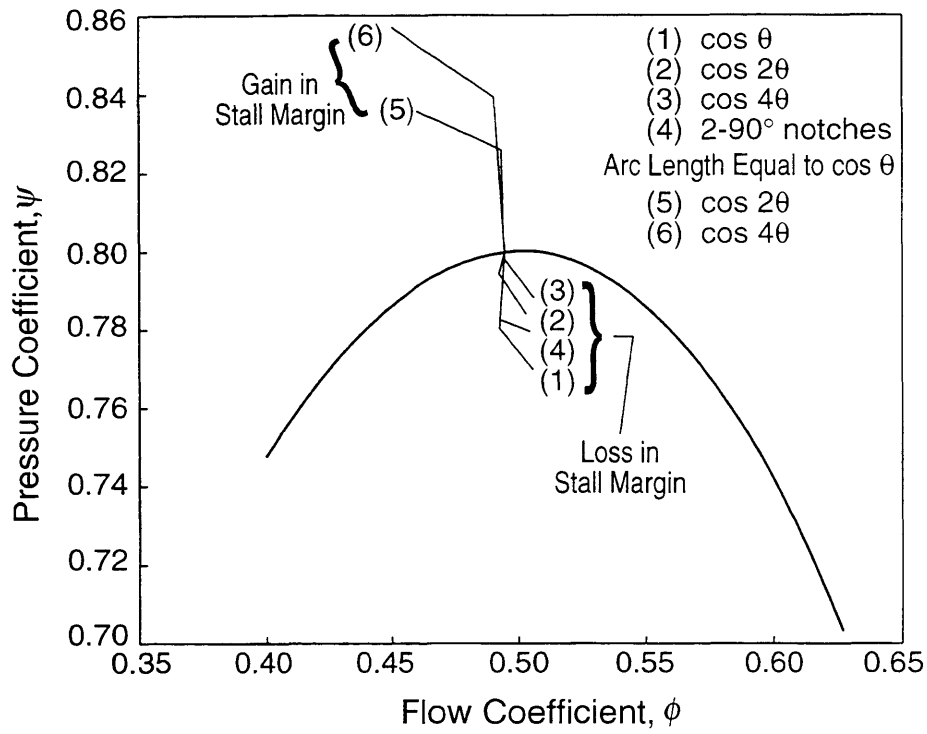

Fig. 27: Effect of circumferential clearance distribution and amplitude on instability point.

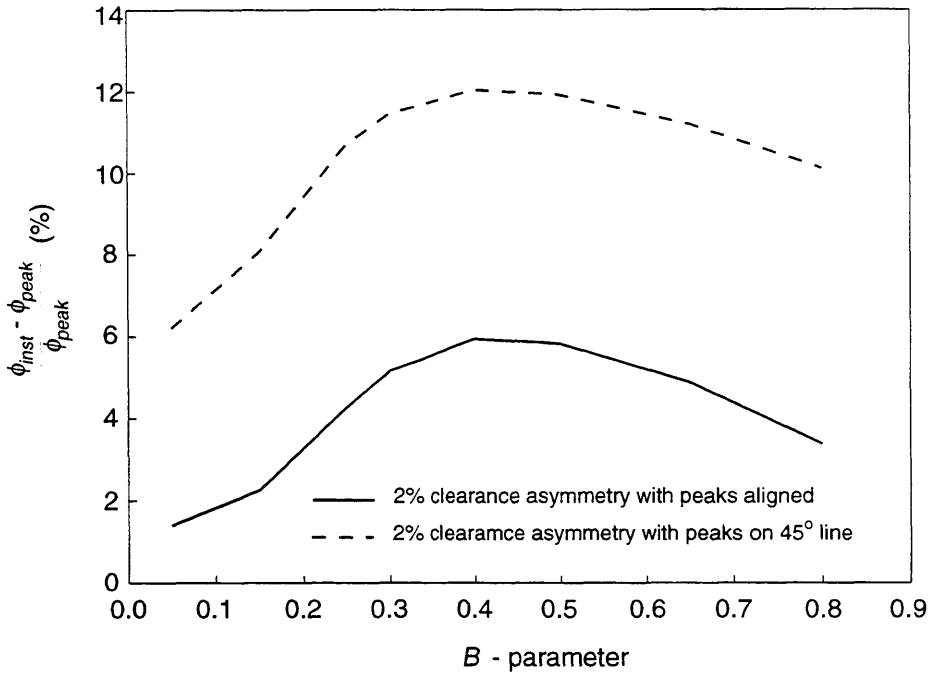

Fig. 28: Change in flow coefficient at instability with B-parameter.

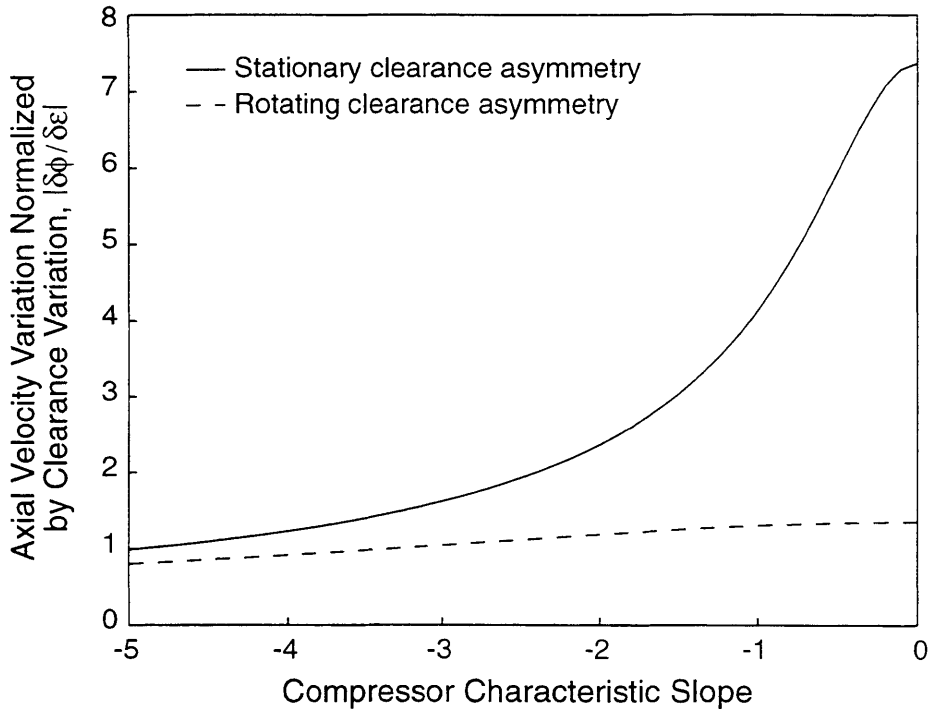

Fig. 29: Magnitude of flow non-uniformity induced by stationary and rotating clearance asymmetries. Parameters of baseline three-stage compressor.

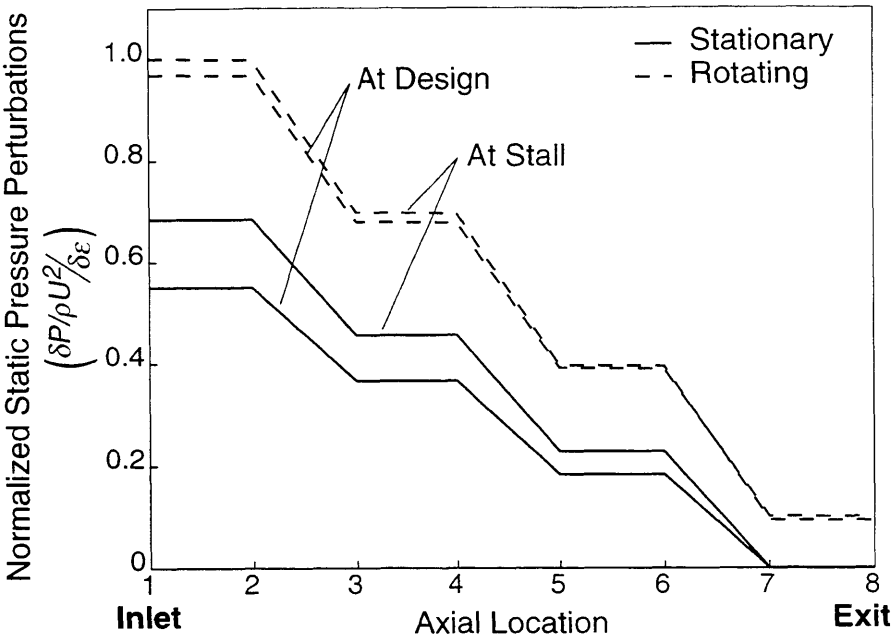

Fig. 30: Static pressure perturbation in a three-stage compressor with stationary and rotating clearance asymmetries.

APPENDIX A: EQUATIONS IN COMPRESSION SYSTEM MODEL

The equations described in this appendix were utilized to determine both the nonlinear steady flow and the stability of this flow to small disturbances. For additional details regarding the development of the equations given here, see Hynes and Greitzer (1987), Longley (1993), and Haynes *et al.* (1994).

The compression system to be modeled is that shown in the schematic of Figure 5. The assumptions utilized to develop the mathematical model are:

Assumptions

- Far upstream inlet conditions to system are uniform and constant
- Two-dimensional, inviscid flow external to the compressor
- Quasi-steady pressure rise across compressor modified by (1) pressure difference required to overcome the inertia of fluid within the blade rows, and (2) a simple model for the loss response of blade rows in an unsteady flow
- Compressor outflow is axial
- Flow in the plenum is spatially uniform and isentropic
- Pressure drop through throttle is quasi-steady with the time-averaged, annulus averaged flow coefficient.

A.1 Steady Background Flow

For steady flow in the compression system shown in Figure 5, the following relations hold.

Upstream Duct:

$$P_{t1}(\theta) = P_{t2}(\theta) \tag{A.1}$$

Compressor:

$$\frac{P_3 - P_{t2}}{\rho U^2} = \psi_i - L_r - L_s - \lambda \frac{\partial \phi}{\partial \theta} \tag{A.2}$$

$$\tau_r \frac{U}{r} \frac{\partial L_r}{\partial \theta} = \bar{L}_r - L_r \tag{A.3}$$

$$\lambda = \sum_{i=1}^{N} \frac{U}{r}\left(T_{r,i}\right) \tag{A.4}$$

where

$$T = \frac{b_x}{U \cos^2 \gamma}$$

The rotor and stator loss are determined using the reaction distribution,

$$\begin{aligned} \bar{L}_s &= L_s = (1 - R)(\psi_i - \psi) \\ \bar{L}_r &= R(\psi_i - \psi) \end{aligned} \tag{A.5}$$

Downstream Duct/Plenum:

$$P_3(\theta) = P_4(\theta) \tag{A.6}$$

Throttle:

$$\frac{P_4 - P_5}{\rho U^2} = \frac{1}{2} k_t \bar{\phi}_3^2 \tag{A.7}$$

The mathematical and physical description of ψ and ψ_i utilized in the present study are given in Appendix B. There the effect of circumferentially non-uniform tip clearance is incorporated through these characteristics.

A.2 Linearized Equations Governing Stability

The dynamical equations for the compression system are linearized by assuming that each variable can be represented as the sum of a mean and a perturbation,

$$f = \bar{f} + \delta f \tag{A.8}$$

After substitution into the governing equations, only first order terms in δ are retained.

Upstream Duct:

The disturbances upstream of the compressor are of potential form and decay exponentially. The disturbance velocity potential for the n^{th}-spatial harmonic is

$$\delta\Phi = f(x)e^{i(n\theta+\omega t)} \tag{A.9}$$

which satisfies

$$\nabla^2\delta\Phi = 0 \tag{A.10}$$

for upstream decaying perturbations. Hence

$$\delta\Phi(x,\theta,t) = a_n e^{|n|(x/r)+i(n\theta+\omega t)} \tag{A.11}$$

The velocity potential is related to the upstream flow coefficient perturbation by

$$\delta\phi = \frac{\partial}{\partial x}(\delta\Phi) = \frac{|n|}{r}\delta\Phi \tag{A.12}$$

The linearized unsteady momentum equation for the flow in the upstream duct can be written

$$\frac{1}{U}\frac{\partial}{\partial t}(\delta\Phi) + \frac{\delta P_t}{\rho U^2} = \text{Constant} . \tag{A.13}$$

Substituting (A.12), at the compressor inlet and invoking the boundary condition of time independent total pressure at the upstream inlet,

$$\left.\frac{\delta P_t}{\rho U^2}\right|_2 = -\frac{1}{|n|}\frac{r}{U}\frac{\partial}{\partial t}(\delta\phi_2) \tag{A.14}$$

Compressor:

Following Hynes and Greitzer (1987), a description of the unsteady flow through the compressor is given by,

$$\frac{P_3 - P_{t1}}{\rho U^2} = \psi_i - L_r - L_s - \lambda \frac{\partial \phi}{\partial \theta} - \frac{\mu r}{U} \frac{\partial \phi}{\partial t} \tag{A.15}$$

$$\mu = \left[\sum_{i=1}^{N} \left(T_{r,i} + T_{s,i} \right) + T_{IGV,i} \right] \frac{U}{r} \tag{A.16}$$

Linearizing this relation yields,

$$\frac{\delta P_3 - \delta P_{t1}}{\rho U^2} = \frac{d\overline{\psi_i}}{d\phi} \delta\phi - \delta L_r - \delta L_s - \lambda \frac{\partial(\delta\phi)}{\partial \theta} - \frac{\mu r}{U} \frac{\partial(\delta\phi)}{\partial t} \tag{A.17}$$

where

$$\overline{\psi_i} = \overline{\psi} + \overline{L_r} + \overline{L_s} \tag{A.18}$$

The blade row unsteady viscous response models employed in the present investigation are, following Haynes et al (1994), simple first order lags which account for the finite time required for the development of loss within the compressor. For the stator, the transient stagnation pressure loss perturbation is given by,

$$\tau_s \frac{\partial(\delta L_s)}{\partial t} = \frac{\partial \overline{L}_s}{\partial \phi} \delta\phi - \delta L_s \tag{A.19}$$

The rotor transient stagnation pressure loss is,

$$\tau_r \left(\frac{\partial(\delta L_r)}{\partial t} + \frac{U}{r} \frac{\partial(\delta L_r)}{\partial \theta} \right) = \frac{\partial \overline{L}_r}{\partial \phi} \delta\phi - \delta L_r \tag{A.20}$$

The loss generation time constants, τ_s and τ_r, are on the order of the blade row flow through time. Equations (A.17) - (A.20) are the linearized equations governing the compressor dynamic response.

Downstream Duct:

In the exit duct, there are both convected vortical disturbances and downstream decaying potential perturbations. For axial exit flow from the compressor through a high solidity (constant leaving angle) exit blade row, the axial momentum equation is,

$$\frac{1}{U}\frac{\partial}{\partial t}(\delta\phi) = -\frac{\partial}{\partial x}\left(\frac{\delta P}{\rho U^2}\right) \tag{A.21}$$

The exit pressure field perturbations must decay axially downstream (i.e. $\nabla^2 \delta P = 0$), hence they will have a form similar to (A.11). Based on this,

$$\frac{\partial}{\partial x}\left(\frac{\delta P}{\rho U^2}\right) = -\frac{|n|}{r}\frac{\delta P}{\rho U^2} \tag{A.22}$$

or, at the compressor discharge,

$$\left.\frac{\delta P}{\rho U^2}\right|_3 = \frac{1}{|n|}\frac{r}{U}\frac{\partial}{\partial t}(\delta\phi_3) \tag{A.23}$$

Equation (A23) determines the perturbation behavior in the exit flow field.

Plenum and Exit Throttle:

For steady flow the static pressure in the plenum is determined by the throttle setting as given in equation (A.7). The flow through the throttle is regarded as quasi-steady, and the flow in the plenum is spatially uniform with pressure and density changes being related by an isentropic relationship (see Greitzer (1981)). Under these constraints, the linearized continuity equation for the plenum is,

$$\left(4B^2 \cdot \frac{L_{total}}{r} \cdot \frac{i\omega r}{U} + \frac{1}{\bar{\phi}_3 k_t}\right)\frac{\delta P_4}{\rho U^2} = \delta\phi_3 \tag{A.24}$$

where the quantity L_{total} is the "effective" compressor length defined as,

$$L_{total} = L_1 + L_2 + \mu r \tag{A.25}$$

and B is as defined in equation (8).

APPENDIX B: FORMULATION OF COMPRESSOR CHARACTERISTICS

In this appendix the mathematical development of the actual and isentropic pressure rise characteristic with clearance asymmetry is presented. Data such as that of Wisler (1985a) and McDougall (1990) show that in general the variation of pressure rise characteristics with clearance is as illustrated in Figure B.1. In this schematic, regions with smaller than nominal clearance are characterized by higher pressure rise, while regions with larger than nominal clearance produce lower pressure rise. The nominal tip clearance pressure rise characteristic has its peak at $(\overline{\phi}_p, \overline{\psi}_p)$.

B.1 Baseline Characteristics

Assume that the pressure rise characteristic can be adequately represented by a generalized cubic polynomial,

$$\psi(\phi) = A\phi^3 + B\phi^2 + C\phi + D \tag{B.1}$$

where the constants are to be determined.

To place the characteristic peak at a point (ϕ_p, ψ_p), the slope of the cubic must be identically zero there, hence

$$\left.\frac{\partial\psi}{\partial\phi}\right|_{\phi_p} = 3A\phi_p^2 + 2B\phi_p + C \equiv 0 \tag{B.2}$$

or, solving for A,

$$A = -\frac{\left(2B\phi_p + C\right)}{3\phi_p^2} \tag{B.3}$$

In addition, at the peak the pressure rise is also known, so substituting (B.3) into (B.1)

$$\psi_p = \tfrac{1}{3}B\phi_p^2 + \tfrac{2}{3}C\phi_p + D \tag{B.4}$$

and solving for D,

$$D = \psi_p - \tfrac{1}{3}\phi_p\left(2C + B\phi_p\right) \tag{B.5}$$

To further reduce the number of free parameters and form characteristics of a realistic nature, a hinge point must also be specified. For the nominal characteristic this is the point $(\overline{\phi}_m, \overline{\psi}_m)$ in Figure B.1. Specification of the hinge allows B or C to be obtained. In the present case it has proven most effective to solve for C in terms of B, hence from (B.1), (B.3) and (B.5) evaluated at some (ϕ_m, ψ_m),

$$\psi_m = -\frac{\left(2B\phi_p + C\right)}{3}\phi_m^3 + B\phi_m^2 + C\phi_m + \psi_p - \tfrac{1}{3}\phi_p\left(2C + B\phi_p\right) \tag{B.6}$$

or solving for C,

$$C = \frac{3\phi_p^2\left(\psi_p - \psi_m\right) - 2B\phi_p\phi_m^3 + 3B\phi_p^2\phi_m^2 - B\phi_p^4}{\phi_m^3 - 3\phi_p^2\phi_m + 2\phi_p^3} \tag{B.7}$$

Therefore, the cubic characteristic passing through a peak at (ϕ_p, ψ_p) and a hinge point at (ϕ_m, ψ_m) is given by equation (B.1) with coefficients A, C, and D specified by (B.3), (B.5) and (B.7) respectively. The constant B was chosen through iteration to obtain the desired characteristic shape.

Once the characteristic is determined it is often useful to compute the radius of curvature at its the peak. Using the definition of radius of curvature, with $\partial\psi/\partial\phi = 0$, the peak radius is,

$$r_p = \frac{1}{\left|\partial^2\psi/\partial\phi^2\right|} = \frac{1}{\left|6A\phi_p + 2B\right|} \tag{B.8}$$

B.2 Characteristics with Tip Clearance Asymmetry

Data indicate that clearance changes affect both the pressure rise and the flow coefficient associated with the peak of the characteristic. The following equations were developed to modulate the peak pressure rise in a manner which depends upon the clearance geometry, the size of the asymmetry, and the sensitivity of the compressor to clearance changes. The quantity $\overline{\psi}_p$ is

the peak pressure rise of the nominal clearance characteristic so that

$$\psi_p = \overline{\psi}_p \cdot \left\{ 1 + \left| \frac{\partial \psi}{\partial \varepsilon} \right| \delta\varepsilon \cdot f(\theta) \right\} \tag{B.9}$$

where $\delta\varepsilon$ = maximum amplitude of the asymmetry

$f(\theta)$ = shape of clearance geometry (e.g. $cos(\theta)$)

$\left| \frac{\partial \psi}{\partial \varepsilon} \right|$ = sensitivity of compressor pressure rise to clearance change (from data)

The asymmetric clearance characteristic peaks must also be shifted to reflect the observation that the higher peaks occur at lower flow coefficients. This was accomplished through shifts of the nominal characteristic peak flow coefficient,

$$\phi_p = \overline{\phi}_p \cdot \{ 1 - k \cdot f(\theta) \} \tag{B.10}$$

where k is determined from data, or by aligning the peaks on a line of specified angle β as shown in Figure B.1. In the latter case the value of k is obtained from

$$k = \frac{\overline{\psi}_p \delta\varepsilon}{\overline{\phi}_p tan(\beta)} \cdot \left| \frac{\partial \psi}{\partial \varepsilon} \right| \tag{B.11}$$

Similarly, in Figure B.1, the hinge point flow coefficient is also shifted by a small amount, hence

$$\phi_m = \overline{\phi}_m \cdot \{ 1 + m \cdot f(\theta) \} \tag{B.12}$$

where m is typically determined by iteration. The shift in the hinge point is in the opposite direction of the peak shift. Also, the hinge point pressure rise is not modulated so $\psi_m = \overline{\psi}_m$.

Combining relations (B.9), (B.10) and (B.12) with the cubic characteristic defined previously, various families of characteristics can be generated as shown in Figure 2.

B.3 Isentropic Characteristics

The isentropic characteristics utilized in this study were formulated to include shifts due to different levels of clearance. For simplicity it will be assumed that the isentropic total-to-static

characteristic is approximately linear (the procedure is similar for other polynomial approximations),

$$\psi_i = E\phi + G \tag{B.13}$$

A nominal compressor design point can be specified at $(\bar{\phi}_d, \bar{\psi}_d)$ with efficiency η. The definition of efficiency utilized here is,

$$\eta = \frac{\bar{\psi}_d}{\psi_i} \tag{B.14}$$

so by combining (B.13) and (B.14),

$$G = \frac{1}{\eta}\bar{\psi}_d - E\bar{\phi}_d \tag{B.15}$$

In addition, it will be assumed that at the design point the slope of the isentropic characteristic is approximately equal to that of the actual characteristic. Therefore,

$$E = \left.\frac{\partial\psi}{\partial\phi}\right|_{\bar{\phi}_d} = 3A\bar{\phi}_d^2 + 2B\bar{\phi}_d + C \tag{B.16}$$

where A, B and C were previously specified for each characteristic in the family.

To determine the efficiency of the compressor at a particular level of clearance, the formulation proposed by Smith (1970) (see also Koch and Smith, 1976) was utilized. Smith's result accounts for both the blockage and tangential force defect in the endwall region. Smith (1970) defines,

$$\eta = \tilde{\eta} \cdot \frac{\left(1 - \frac{\delta_h^* + \delta_t^*}{h}\right)}{\left(1 - \frac{\nu_h + \nu_t}{h}\right)} \tag{B.17}$$

where cascade or midspan efficiency is denoted by $\tilde{\eta}$, while δ^* and ν represent the endwall flow

displacement thickness and tangential force defect respectively. In the worst case, the endwall flow will provide no tangential force on the blading ($F_u = 0$), hence from Smith (1970),

$$v_h = \frac{1}{r_h \tilde{F}_{uh}} \int_{r_h}^{r_h+\delta_h} (\tilde{F}_u - F_u) r dr = \frac{1}{r_h} \int_{r_h}^{r_h+\delta_h} r dr \tag{B.18}$$

so,

$$v_h \approx \delta_h$$

and similarly at the tip,

$$v_t \approx \delta_t$$

As a first approximation based on data, assume,

$$\begin{aligned} v_{h,t} &\approx \delta_{h,t} \approx 1 \text{ clearance height} \\ \delta^*_{h,t} &\approx 3\delta_{h,t} \approx 3 \text{ clearance heights} \end{aligned} \tag{B.19}$$

Therefore, using (B.19), (B.17) the efficiency is,

$$\eta \approx \tilde{\eta} \cdot \frac{\left(1 - \frac{6\varepsilon}{AR}\right)}{\left(1 - \frac{2\varepsilon}{AR}\right)} \tag{B.20}$$

where the clearance has been normalized by chord, and AR is the blade aspect ratio. Note that with clearance asymmetry the efficiency will vary around the annulus since ε is a function of θ.

In summary, the isentropic characteristics with clearance asymmetry are obtained by combining (B.13) and (B.15),

$$\psi_i = (\phi - \bar{\phi}_d) \left.\frac{\partial \psi}{\partial \phi}\right|_{\bar{\phi}_d} + \frac{1}{\eta} \bar{\psi}_d \tag{B.21}$$

where the derivative is given by (B.16) and efficiency is approximated from (B.20).

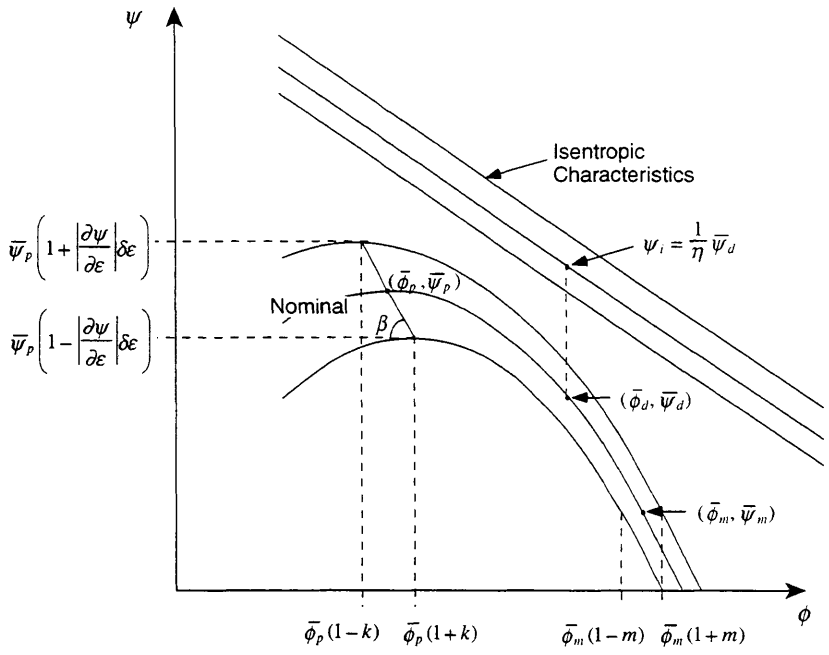

Fig. B.1: Schematic of actual and isentropic compressor pressure rise characteristics.

APPENDIX C: ANALYSIS OF ROTATING CLEARANCE ASYMMETRY

In this appendix a linearized description is given of the response of a compressor to a rotating clearance asymmetry.

Upstream Duct:

As a result of the rotating clearance non-uniformity, the total pressure upstream of the compressor will vary in time. Using Eq. (A.14) the unsteady changes in inlet total pressure are

$$\frac{\delta P_{t,inlet}}{\rho U^2} = \frac{1}{|n|}\frac{r}{U}\frac{\partial \delta\phi}{\partial t} \tag{C.1}$$

with the n^{th} harmonic of $\delta\phi$ given by (A.11) and (A.12) as

$$\delta\phi_n = \frac{|n|}{r} a_n \, e^{|n|(x/r)+i(n\theta+\omega t)} \tag{C.2}$$

so

$$\frac{\delta P_{t,inlet}}{\rho U^2} = \frac{-i\omega r}{|n|U}\delta\phi_n \tag{C.3}$$

where ω is the disturbance frequency associated with the rotating asymmetry. For an n-lobed rotating asymmetry,

$$\omega = n\frac{U}{r} \tag{C.4}$$

Substituting (C.4) into (C.3),

$$\frac{\delta P_{t,in}}{\rho U^2} = -i\delta\phi_n \tag{C.5}$$

Downstream Duct:

The pressure distribution downstream of the compressor will also vary in time. Using the

exit condition of constant leaving angle, Eq. (A.23) gives the unsteady static pressure variation as

$$\frac{\delta P_{exit}}{\rho U^2} = \frac{1}{|n|}\frac{r}{U}\frac{\partial \delta\phi}{\partial t} \tag{C.6}$$

and using (C.2) and (C.4),

$$\frac{\delta P_{exit}}{\rho U^2} = i\delta\phi_n \tag{C.7}$$

Compressor:

The linearized equation for the compressor response with a rotating clearance asymmetry is Eq. (4) with an additional term related to the unsteady response of the compressor flow field.

$$\frac{\delta P_{exit} - \delta P_{t,inlet}}{\rho U^2} = \frac{\partial \psi}{\partial \phi}\delta\phi + \frac{\partial \psi}{\partial \varepsilon}\delta\varepsilon - \lambda\frac{\partial \delta\phi}{\partial \theta} - \frac{\mu r}{U}\frac{\partial \delta\phi}{\partial t} \tag{C.8}$$

Substituting the inlet and exit duct equations (C.5) and (C.7) gives

$$\lambda\frac{\partial \delta\phi}{\partial \theta} + \frac{\mu r}{U}\frac{\partial \delta\phi}{\partial t} - \frac{\partial \psi}{\partial \phi}\delta\phi + 2i\delta\phi = \frac{\partial \psi}{\partial \varepsilon}\delta\varepsilon \tag{C.9}$$

and using Eqs. (C.2) and (C.4),

$$\delta\phi\left\{2i + in(\lambda+\mu) - \frac{\partial \psi}{\partial \phi}\right\} = \frac{\partial \psi}{\partial \varepsilon}\delta\varepsilon \tag{C.10}$$

or,

$$\delta\phi = \frac{\frac{\partial \psi}{\partial \varepsilon}\delta\varepsilon}{in(\lambda+\mu) + 2i - \frac{\partial \psi}{\partial \phi}} \tag{C.11}$$

Equation (C.11) gives the flow non-uniformity ($\delta\phi$) induced by a rotating asymmetry ($\delta\varepsilon$). As compared to Eq. (7) for the stationary asymmetry, new terms have been introduced in the

denominator; one is related to unsteady flow in the compressor and the other to the unsteady flow in the inlet and exit ducts. By taking the ratio of Eq. (7) to Eq. (C.11) and assuming that the sensitivity to clearance change ($\partial\psi/\partial\varepsilon$) and the clearance variation ($\delta\varepsilon$) are the same for the rotating and stationary asymmetries, we obtain

$$\frac{\delta\phi_{stat}}{\delta\phi_{rot}} = \frac{in(\lambda+\mu)+2i-\dfrac{\partial\psi}{\partial\phi}}{in\lambda-\dfrac{\partial\psi}{\partial\phi}} \tag{C.12}$$

and near the peak of the characteristic ($\partial\psi/\partial\phi \approx 0$),

$$\frac{\delta\phi_{stat}}{\delta\phi_{rot}} = \frac{n(\lambda+\mu)+2}{n\lambda} \tag{C.13}$$

These results show that a stationary clearance asymmetry induces a greater axial velocity non-uniformity than that obtained if the same asymmetry were rotating.